Practical Trials of Fiber Optical Gyroscope Based Inertial Navigation System

Tim Djärf

LUND
UNIVERSITY

Department of Automatic Control

MSc Thesis
TFRT-6196
ISSN 0280-5316

Department of Automatic Control
Lund University
Box 118
SE-221 00 LUND
Sweden

Printed in Sweden by Tryckeriet i E-huset
Lund 2023

Abstract

There exists a need for inertial navigation systems within a multitude of applications, such as drones, unmanned vehicles, and guidance systems. Saab produces gyroscopes for stabilization purposes, but the gyroscopes could also be used as part of an inertial navigation system. This thesis investigate the viability of using the hardware and software that Saab already uses, with the addition of accelerometers which is sourced from Safran sensing technologies; as components in a inertial navigation system.

A prototype inertial navigation system has been built, and a navigation algorithm has been implemented. The prototype has been calibrated on both sensor and system level. The sensors have been verified to lie well within the manufacturers specifications.

It is possible to use the current hardware used by Saab for navigation purposes, as verified by measuring timing and computational load of the prototype system. However, there still exist a numerical error for the velocity and position calculation which requires additional development. Development and testing of the navigation unit will have to be continued outside the scope of this master's thesis to determine how viable the system could be as a product used in actual applications.

Sammanfattning

Det finns ett behov av tröghetsnavigeringssystem för flertalet applikationer, så som drönare, obemannade farkoster och styrsystem för navigering. Saab producerar i dagsläget gyroskop som säljs för stabilisering, men gyroskopen skulle också kunna användas som komponenter i ett tröghetsnavigeringssystem. Detta examensarbete undersöker om det är möjligt att använda den hårdvara och mjukvara som Saab redan använder, som komponenter i ett tröghetsnavigeringsystem.

En prototyp av ett tröghetssystem har byggts, och en algoritm för navigation har implementerats. Prototypen har kalibrerats både på sensornivå och som en komplett enhet. Det har bekräftats att alla sensorer ligger inom tillverkarnas specifikationer.

Det är möjligt att använda den nuvarande hårdvaran som Saab använder för navigation, vilket har verifieras genom mätning av tiden för navigationsalgoritmen och genom mätning av processorns användande. Dock så existerar det fortfarande ett numeriskt fel för beräkningen av hastighet och position vilket kommer kräva ytterligare utvecklingstid. Utveckling och testing av enheten för navigation kommer behöva fortsättas utanför ramen av detta examensarbete för att bekräfta möjligheterna att ta prototypen till en produkt som kan användas.

Acknowledgement

This thesis marks the end of my time as a student, an journey which has taken more time than expected. I am happy to have made this journey, and maybe even happier that it is over. During my time as a student at Lund university I have learned a multitude of life skills as well as I have received a great education within computer science. I will continue to take great pride in my education as time goes on.
I would also like to extend my thanks to a number of people.

I would like to thank my academic supervisor, Bo Bernhardsson, for the his insightful discussions on navigation and for all notes I received on my report, the work would not have come as far as this without your support. I would also like to thank my examiner, Karl-Erik Årzén.

I would also like to thank my company supervisor, as well as Daniel Månsson and Björn Holgersson for introducing me to Saab as well as the FOG group. Your company and support with anything gyro has been vital for making this thesis possible. I would also like to extend a thank you to all other colleges for the warm welcome and for making any time spent at the office enjoyable.

During my studies I have enjoyed the privilege to advocate for student rights and take part in the the work of Teknologkåren and LUS. I would like to thank all those that I have met during my time as a student representative and volunteer, I will remember this time fondly. Even all those meetings that went on well into the night.

I would also like to thank my family and my fiances family for their unfaltering support during these years, I could not have done it without you. My brothers for always laughing with me. My mother and father for always listening.

Lastly, I would like to thank my fiancee. You make me want to be the best me, pushing on even when life is hard.

"*A journey of a thousand miles begins with a single step*" - Laozi

Contents

1. Introduction **12**

2. Background **13**
2.1 Goals . . . 13
2.2 Methodology . . . 13
2.3 Restrictions . . . 14

3. System components **15**
3.1 Gyroscope . . . 15
3.2 Accelerometer . . . 15
3.3 Inertial measurement unit . . . 15
3.4 Inertial navigation system . . . 16

4. Construction **17**

5. Technical background **19**
5.1 Mathematical model . . . 19
5.2 Navigational model . . . 19
5.3 Coordinate frames . . . 21
5.4 Moving between coordinate frames . . . 22
5.5 Error classification . . . 24

6. Calibration **27**
6.1 Sensor calibration . . . 31
6.2 Cross-axis . . . 43

7. Alignment **44**

8. Software **47**
8.1 Software overview . . . 47
8.2 Software implementation . . . 48

9. Results **49**

10. Discussion **52**
10.1 Ethical considerations . . . 52
10.2 Future work . . . 53

A. P.G Savage model **54**

B. Saab 8088000-4xx gyroscope **58**

C. Safran accelerometer **60**

Bibliography **65**

Abbreviations and mathematical symbols

IMU	Inertial Measurement Unit
INS	Inertial Navigation System
GNSS	Global Navigational Satellite System
GPS	Global Positioning System
MEMS	MicroElectroMechanical System
FOG	Fiber Optical Gyroscope
ARW	Angular Random Walk
VRW	Velocity Random Walk

$\times$	cross-product
$\equiv$	equivalence
$\approx$	approximately

1

Introduction

Inertial navigation systems, INS, enable navigation using no external input, useful for applications where there might be interference when using other kinds of navigation systems. Boats were traditionally navigated using the sun and stars as reference, which were easily hindered by a cloudy day. The development and now common usage of gyroscopes and accelerometers as INS stem from this very problem; how can one construct a system for navigation using as little external input as possible [Tazartes, 2014].

Fiber optical gyros, FOGs, were proposed as early as 1976. They are lightweight and small, and allow for operations in in a wide range of applications [Vali and Shorthill, 1976]. FOGs are however affected by temperature changes, as well as angular random walk. There are computational methods and filtering techniques that mitigate these issues; however, reducing errors remain an area of ongoing active research [Noureldin et al., 2001] [Morris et al., 2022].

Saab currently produces FOGs for stabilisation purposes, these gyroscopes are in turn mounted in a wide array of applications [Saab AB, 2022]. Saab also uses inertial navigation systems with other types of gyroscopes. This thesis aims to marry these two section within Saab, the fiberoptical gyros and the navigation, and test the limitations of an INS which uses FOGs produced by Saab. This thesis will examine the performance of such a system and also determine if an INS using FOGs can perform in such a way that it can be used in actual applications.

The system will be limited to terrestrial navigation and constructed as a prototype, both in terms of durability and test range.

2

Background

An inertial navigation system should provide the user of the system with movement information. Commonly the INS system outputs velocity, position and attitude. Velocity is the change in position in relation to the local area. Position is commonly expressed as the location where the system is in relation to Earth, and attitude is the change in orientation of the craft in relation to some static reference frame. For example a car could be driving along the E6 outside Lund; the car has a velocity of $100 km/hr$, the position can be expressed as the city the car is currently passing through and the attitude would then express the direction in which the car is driving; going north and maybe up a hill.

2.1 Goals

The goals of this thesis are to answer the following questions.

- **RQ1**: Can the existing hardware within Saab be used for navigation?
- **RQ2**: For how long is an inertial navigation system with the provided hardware trustworthy?
- **RQ3**: What, if any, changes need to be realized in hardware and software to produce a working navigation system?

The research questions were selected in discussion with Saab and is a based on hardware and competence available.

2.2 Methodology

The work during this thesis can be divided into multiple distinct parts. Based on the research questions there is a need for a hardware platform on which the navigation algorithm can be tested.

First, a theoretical foundation was laid down for how an INS system works and what parameters are suitable to use for measuring performance. The theory has in part been provided by internal resources at Saab and through previous academic work, and details the sensors, inertial navigation and the errors related to the two. The theory also details the mathematical background for the navigation algorithm, as well as the algorithm used. The thesis draws from current practise within the field and within the company to produce results that can be used for future work and comparisons to current systems.

Secondly, Saab provided a configuration of hardware that was to be examined. The sensors have been measured in reference to the manufacturers specifications to determine the performance of the individual sensor. A construction and a software design was proposed for how an inertial navigation system could be built from the provided components. Then, a prototype was built according to the proposed design. The hardware design and the prototype allowed for trials of the performance of the system but will also serve

as a reference for future constructions. The construction utilizes experiences within Saab, using existing implementations and solutions to increase comparability to other existing systems and future implementations. The prototype was initially run with existing, verified, software to calibrate the individual sensors. Then, with each sensor calibrated, the unit was calibrated as a complete sensor package.

Third, the selected algorithm was implemented. The software was built as an adaptation of existing Saab software, with the aim to reuse as much code as possible, and keep compatibility for other sensors and implementations that Saab already has.

Lastly, the inertial navigation system was tested. Primarily; the INS was tested during standstill to determine timing of both the algorithm and the output. The system was also tested for drift, during standstill. The testing was adapted during the thesis to provide relevant data so that development could be continued. As an example, there is simply no need to do movement testing when the drift is unreasonably large during standstill testing.

2.3 Restrictions

Some restrictions have been selected to make the project possible to realize; these restrictions also determine the scope of the results.

The thesis will draw as much as possible from existing hardware and software within Saab. Not only will it decrease development time, but it will also provide backwards compatibility with existing Saab solutions. The system built will be a prototype, both in terms of durability and construction quality. The hardware used has a wide range of operation in terms of temperature, and limits have been introduced to decrease the time for calibration and testing. No additional input will be used for the system, information may be input during startup, but after start, only the sensor packet is used for input. Aided inertial navigation systems introduce additional complexity and depending on the aid, additional calculations. The prototype should be as self contained as possible, meaning it will be movable and require little setup when used. The alignment at startup of the system will not determine heading in relation to Earth, it will be assumed that the system is oriented correctly along the Earth. The system will also have the location; longitude, latitude, and height, input before starting. This decreases the computations required during startup and system alignment. The system built is intended to be used in terrestrial applications, and testing will only be done in relation to Earth. Testing will also be limited to ground motions; by the use of a cart which the navigation system can be moved with. This restriction also determine what forces that needs to be considered. According to Paul G. Savage the divergence characteristics of the vertical is not pronounced for tracking durations shorter than 5 minutes. All tracking must be limited to a maximum of five minutes; otherwise the system will require some kind of altitude compensation, such as a barometric altimeter [Savage, 1997].

3

System components

This section provides a technical introduction to the different components of the system and how they work and interact with each other.

3.1 Gyroscope

During this thesis, three fiber optical gyroscopes have been used. The gyroscopes follow the specification in Appendix A.

A gyroscope measures angular velocity, the rate of change around a rotational axis. Fiber optical gyroscopes measure the Sagnac effect, the interference between two beams of light which have undergone a rotation. Gyroscopes are however affected by errors, some which can be limited by calibration. The errors and the calibration of gyroscopes will be presented later in this report.

3.2 Accelerometer

For this thesis, three single axis MEMS (microelectromechanical systems) capacitive accelerometers have been used, following the specification provided in Appendix C. The accelerometers have been measured and follow the specification.

An accelerometer measures specific force acceleration. This implies that an accelerometer with its measurement axis, seen as a vector towards the center of the Earth, will measure gravity and centrifugal force for that position on Earth. In the same manner an accelerometer in inertial space will measure zero. MEMS accelerometers are often composed of a known mass held in space with the use of some force. When the sensor is moved; the mass is displaced a distance relative to the force of the movement. Measuring that displacement and performing some calculations allow the sensor to output a reading of acceleration. The accelerometer suffers from errors, some which can be limited by calibration. The errors and the calibration of the accelerometers will be presented later in this report.

3.3 Inertial measurement unit

An inertial measurement unit, IMU, is the measurement instrument of an inertial navigation system. An IMU consists of different instruments to measure movement or relations between the system and the world. Accelerometers, gyroscopes, magnetometers, altimeters and GNSS (Global Navigation Satellite System) are all instruments that can be used within an IMU. The selection of instruments depends on the use case for the IMU.

During this thesis an IMU is built consisting of three accelerometers and three gyroscopes. An inertial measurement unit suffers from the same issues as its respective sensors, making sensor selection an important design step when designing a navigation system. The inertial measurement unit also has to be calibrated as a unit to compensate for mounting errors, which depend on the mounting hardware used. The calibrations performed for IMU will be presented later in this report.

3.4 Inertial navigation system

An inertial navigation system, INS, consists of an IMU as well as some sort of processing unit. As the system is unaided, it does not receive any additional input after starting. In comparison an aided system might cross-reference its measured position against a GPS sensor. It is also possible to improve the accuracy of a navigational system with mathematical limitations. For example, a navigation system used in a car could be limited in a way where all sideways motion has to be accompanied with a forward motion. This limit is reasonable for a car as it has to move forward to perform a turn.

The processing unit has to read the measured data from the IMU and calculate the relevant navigation data, which can be output either to some other system or as information to a pilot. The processing unit could also be part of some other system where additional computations are required.

4

Construction

This section details how the INS has been built. The gyroscopes used are made by Saab and belongs to the 8088000-4xx family. They are produced and calibrated in-house. The accelerometers used are produced by Safran Sensing Technologies, model MS1010L 10g. The gyroscopes and accelerometers are grouped and mounted in pairs, as seen in Figure 4.1. Each accelerometer is denoted with an 'A' and a number and each gyroscope is denoted with a 'G' and a number. Each respective pair of an accelerometer and a gyroscope is given the same number. Each pair is mounted to measure the change in angle around a vector as well as the acceleration parallel to the the same vector. The three measured vectors are intended to be orthogonal in respect to each other, but there is need to introduce compensation due to imperfections in the mounting hardware.

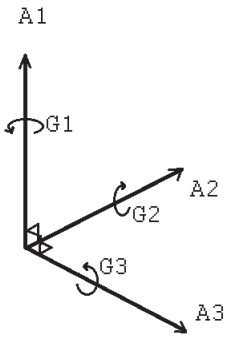

Figure 4.1 Illustration of sensor mounting in respect to each other. Accelerometers are denoted with an 'A' and gyroscopes with a 'G'. Each sensor is also denoted with a number to differentiate the sensors from one another.

All gyroscopes and accelerometers are powered by a power card produced by Saab. These parts were fitted, as a unit, into existing Saab mounting gear to provide backwards compatibility with existing test equipment and mounting solutions. The unit can be fed a supply voltage, and utilizes the power card to separate the power lines between the analog and the digital parts of the system to limit noise between the different parts. All cables used during the thesis have also been kept as short as possible to minimize

interference. This unit returns the sensor data to be read by the processing unit.

The processing unit consists of an AD converter and a processor prototype board. The processor prototype board consists of a processor and some common peripherals; such as pins, USB-connectivity, and LEDs, that can be used for development. Another useful part of the processor prototype board is that it contains a separate processor which can be used for calculations and offloading the main CPU. The processor prototype board has the option to connect an add-on card, this allows the processor to connect to other systems using a 9-pin dsub port as well.

The AD converter reads the voltage levels from the sensors in the IMU, which it converts and sends as a digital signal to the processor through serial port communication. The processor also receives the temperature levels of the sensors as a voltage level which it converts on the processor board using an internal ADC.

The processor converts the digital signals to angular rate, specific force and temperature, which can be used as input for the navigational algorithms. The processor calculates the navigation data and sends out the result on either USB or RS-232.

5

Technical background

This section describes any background information that might be needed to understand the system and how the navigational algorithm works.

5.1 Mathematical model

A well-defined mathematical model offers a comprehensive understanding of the system and its components function in relation in relation to one another. It also facilitates ease of comprehension and enables comparison with other systems. The model employed in this paper was devised bu Paul G. Savage and has been replicated in Appendix A for the reader's convenience [Savage, 2015]. The mathematical model is constructed on the basis of three mutually perpendicular unit vectors, which are used to denote the system and surrounding space. The three vectors construct a Cartesian coordinate system, which is right-handed. A positive rotation is the counter-clockwise motion of a vector being spun around its rotational axis.

The system can be represented in two ways, either with the use of directional cosines or quaternions. The representations give the same accuracy and only differ in formulation and calculations [Savage, 2015]. During this thesis the system has been represented using directional cosines for ease of understanding.

5.2 Navigational model

The navigation during this thesis is terrestrial in nature, as such the largest forces acting on the system will be those of the navigational system moving, and the Earth. Therefore, we define a multitude of parameters in relation to Earth to know what the system should consider when navigating. The simplest navigation system would ignore any forces imparted by Earth, except for a single approximation of the gravity of Earth. In contrast, a navigation systems that are to be used over large distances and during longer running times require a accurate model of the Earth.

One such model of Earth is the WGS-84 Earth model, which compensates for the flattening of Earth to produce a oblate spheroid. WSG-84 defines position in relation to Earth as ECEF coordinates, with the origin at the center of mass for the Earth, the Z-axis directed the IERS reference pole, which is close to the north pole. The X-axis is directed at the IERS reference meridian which lies close but not overlapping the Greenwich meridian, originating at the center of Earth and normal to the Z-axis. The Y-axis then completes a right-handed orthogonal system by being a 90° positive rotation around the Z-axis based on the X-axis [National Geospatial-Intelligence Agency, 2014]. The WSG-84 model of the Earth and the axes can be seen below in Figure 5.1, with the three orthogonal axes drawn in reference to Earth. For ease

of understanding, the IERS reference poles will simply be referred to as the "north" or the "south" pole. In the same manner the IERS reference meridian will be referenced to as the Greenwich meridian in this report. WSG-84 also defines earth rate, and gravitational constants which will be used as parameters in the navigational algorithm. These constants can be seen below in Table 5.1.

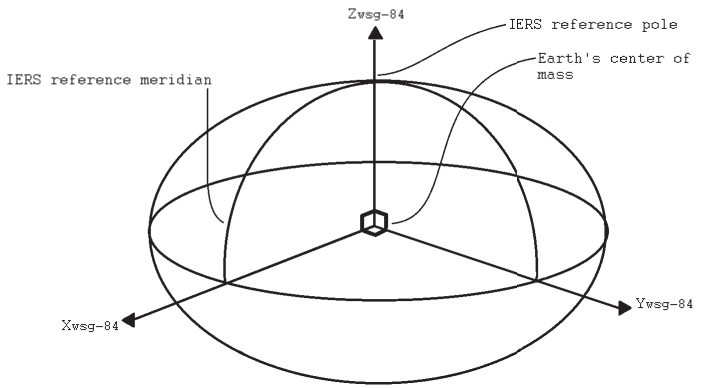

Figure 5.1 WSG-84 Earth model with coordinate axes. The oblateness of the Earth has been exaggerated.

The physical constants defined by WSG-84 that have been used during this thesis are as follows:

Table 5.1 WSG-84 constants.

Earth's semi-major axis	a	$6378.137km$
Earth's semi-minor axis	b	$74747km$
Inverse of Earth's flattening	f	$1/298.257223563$
First Eccentricity Squared	e	$6.694379990141 \cdot 10^{-3}$
Earth's angular velocity	ω	$72.92115 \cdot 10^{-6} rad/s$
Normal gravity at the Equator	γ_e	$9.7803253359 m/s^2$
Normal gravity at the poles	γ_p	$9.8321849379 m/s^2$

The variation in the thickness of the Earth also produces variation in the gravity, such variations have been ignored during this thesis, but variations based on position have been included.

WSG-84 calculates the local gravity as follows.

$$\gamma = \gamma_e \frac{1 + k\sin^2(\phi)}{\sqrt{1 - e^2\sin^2(\phi)}} \tag{5.1}$$

where

$$k = \frac{b\gamma_p}{a\gamma_e} - 1$$

ϕ = geodetic latitude

For the sake of this thesis the Earth has been approximated as a sphere, with using the Earth's semi-major axis from WSG-84 for both axes.

5.3 Coordinate frames

For navigation, the use of coordinate frames is utilized. These coordinate frames relate the system to the local area of navigation, and the local area of navigation to the Earth. The INS should allow for transformation between these coordinate frames to provide relevant information to the user of the system. For example, the displacement of the system might be expressed in the navigational frame, or the Earth frame. Both express the position of the craft but it might be more interesting for a pilot to know changes in longitude and latitude; rather than meters of displacement from the starting point of the system. Therefore, transformation matrices are utilized to transform coordinates from one frame to another.

The frames utilized for navigation are as follows:

Body frame

{X, Y, Z} = {Upward, Rightward, Forward}
This coordinate frame provides context to the changes in position for the body frame of the system as movements in the three axis of the craft. The gyroscopes and accelerometers are mounted along these three axes as seen in Figure 5.2 below. The accelerometers are denoted with an 'A' and a number and the gyroscopes are denoted with a 'G' and a number. Each sensor pair, an accelerometer and a gyroscope with the same number, can also be referred to as an axis in the body frame. The axes in the body frame is referred to as X_{body}, Z_{body} or Y_{body} for sensor pair 1, 2, and 3 respectively.

Navigation frame

{X, Y, Z} = {North, East, Down (as local gravity vector)}
The navigational plane corresponds to the local area of the craft. The navigational frame is sometimes refereed to as the local plane. The navigation frame is parallel to Earths surface, with two axes aligned toward north and east of the Earth frame. This frame assumes that Earth's surface can be approximated as flat.

Earth frame

For the Earth frame the WSG-84 model is used. Position in relation to Earth can be expressed in multiple ways. WSG-84 utilizes Cartesian coordinates where position in relation to Earth is given as three coordinates. This system is called Earth Centered Earth Fixed, ECEF. The position can then be viewed

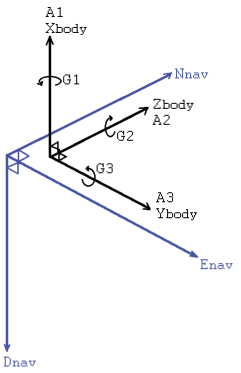

Figure 5.2 Body axes of a navigation system expressed as a Cartesian coordinate system, with positive rotation for each axis, in relation to a navigational frame. The body frame illustrated in black and the navigational frame in blue.

as a vector from the center of the Earth to the position of the craft. For example, Lund University main building is located at $x = 3506901m$, $y = 822106m$, $z = 5246095m$. Position on Earth can also be defined as angles from a point. This system uses the crossing of Earth's meridian and the Greenwich line as the starting point. The position is then expressed as the change in angle along the surface of the Earth. The position is then expressed in longitude, the angle in west-/eastward direction from the Greenwich line, and latitude, the angle in south-northward direction from the Earth's meridian, and height. The height is in reference to Earth's surface. A craft on the ground will have height 0. This notation is called geodetic coordinates, and is commonly used for position during navigation. Once again, the Lund University main building is located at 55°42'21"N 13°11'36"E, which is formatted as degrees, minutes, and seconds; where sixty minutes is one degree, and sixty seconds is one minute. The location of the main building then corresponds to $55 + \frac{42}{60} + \frac{21}{3600} = 55.70583°$ North of the equator and $13 + \frac{11}{60} + \frac{36}{3600} = 13.19333°$ East of the Greenwich line. Using these values as well as the height of the system in relation to Earth's surface one can determine the position in relation to the center of Earth. Either of these three, x, y, and z, or latitude, longitude, and height can be used for describing the navigational frame in relation to Earth.

5.4 Moving between coordinate frames

For this thesis direction cosine matrices have been used to relate the different navigational frames. For a point expressed in a Cartesian coordinate system, the transformation to another coordinate system can be expressed as a rotation of the point around each axis and a translation motion. Each individual rotation can be expressed as its own rotational matrix, which either can be applied individually or as a single matrix. The order of the rotations matter, and the reference frame used to describe the rotation needs to be consistent. For example. if the craft experiences a positive 90° roll and a positive 90° pitch around its own axes, the orientation can vary greatly depending on the representation. In Figure 5.3, a craft first

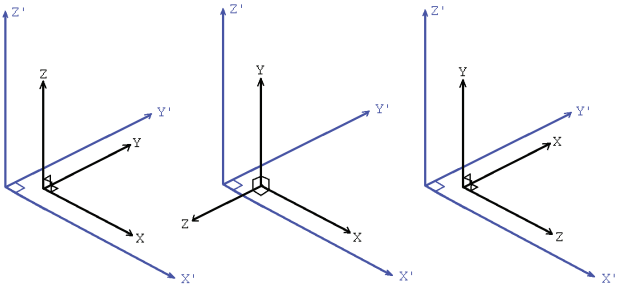

Figure 5.3 A body, in black, rotated 90° around the x-axis of the body and then 90° around the y-axis of the body in an Cartesian coordinate system, illustrated in blue.

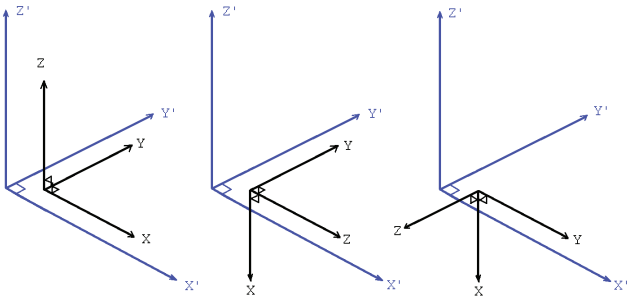

Figure 5.4 A body, in black, rotated 90° around the y-axis of the body and then 90° around the x-axis of the body in an Cartesian coordinate system, illustrated in blue.

experiences a positive rotation around the x-axis of the craft, pitching upwards. The craft then experiences a roll, a positive rotation around the y-axis of the craft. In Figure 5.4, a craft experiences the roll first and then the pitching motion. The final attitude of the craft is vastly different, and care should be taken that the rotation order is kept consistent across all coordinate systems.

Mathematically; the transformation matrices used during the thesis can be described as below. Using ψ for yaw, ϕ for roll, and θ for pitch, implying a rotation around the system's z-axis, a rotation around the system's y-axis, and a rotation around the system's x-axis respectively. All these rotations are to be viewed from the point of view of the body frame.

$$\begin{bmatrix} x' \\ y' \\ z' \end{bmatrix} = R_\phi R_\psi R_\theta \begin{bmatrix} x \\ y \\ z \end{bmatrix} = R \begin{bmatrix} x \\ y \\ z \end{bmatrix} \tag{5.2}$$

where

$$\begin{bmatrix} \cos\phi & -\sin\phi & 0 \\ \sin\phi & \cos\phi & 0 \\ 0 & 0 & 1 \end{bmatrix} \begin{bmatrix} 1 & 0 & 0 \\ 0 & \cos\psi & -\sin\psi \\ 0 & \sin\psi & \cos\psi \end{bmatrix} \begin{bmatrix} \cos\theta & 0 & \sin\theta \\ 0 & 1 & 0 \\ -\sin\theta & 0 & \cos\theta \end{bmatrix} = R_\psi R_\phi R_\theta = R$$

$$\Leftrightarrow \tag{5.3}$$

$$\begin{bmatrix} \cos\phi\cos\theta - \sin\phi\sin\theta\sin\psi & -\sin\phi\cos\psi & \cos\phi\sin\theta + \sin\phi\cos\theta\sin\psi \\ \sin\phi\cos\theta + \cos\phi\sin\theta\sin\psi & \cos\phi\cos\psi & \sin\phi\sin\theta - \cos\phi\cos\theta\sin\psi \\ -\sin\phi\cos\psi & \sin\psi & \cos\theta\cos\psi \end{bmatrix} = R$$

It is then possible to calculate the change in angle in reference to the navigational frame as

$$\phi = \arctan\frac{-R_{12}}{R_{22}} \tag{5.4}$$

$$\theta = \arcsin R_{32} \tag{5.5}$$

$$\psi = \arctan\frac{-R_{31}}{R_{33}} \tag{5.6}$$

This description of motion is know as intrinsic rotations, in the model called Tait-Bryan angles [Markley and Crassidis, 2014].

The INS will continuously calculate the transformation matrices between the body and the navigational frame, and the navigational and Earth frame. This allows the location and attitude of the craft to be expressed in the different navigational frames during runtime. It also allows for the system to output the change in angle for the system as angular change in relation to the starting attitude of the craft.

5.5 Error classification

All sensors used during this thesis have errors, some which can be compensated for. The errors are as follows for the sensors.

Bias offset

The bias offset for a signal is a deviation from the expected true value, either as $^\circ/h$ or m/s^2 depending on the sensor. The bias for gyroscopes and accelerometers has been limited by calibration in this thesis. The measured bias is input into the system to be subtracted continuously from the raw sensor data [Woodman, 2007] [Anon, 2014].

Bias instability

Bias instability is the deviation from the bias offset for a sensor not affected by shock, temperature or vibration. The bias offset of a sensor could be removed completely, bringing the sensor output exactly to

the sensor measured value. With the offset removed, any variation on the signal is called bias instability. It is not possible to compensate for bias instability by sensor calibration, and the instability is a factor worth noting when selecting sensors. Bias instability is either measured in $^\circ/h$ or mg, and a lower value is better [Anon, 2014].

Random angular/velocity walk

The sensors are also affected by white noise, commonly referred to as random walk. As the sensors output measurements the data will fluctuate randomly, this effect can be measured but not compensated for on sensor level [Jurado et al., 2019] [Anon, 2014]. As the sensor is sampled at a high rate, fluctuations in the measured signal will make it seem like the sensor is moving. As seen in the bottom graph in Figures 6.1, 6.2, and 6.3, when the signal is averaged over many signal samples there is still a deviation from the actual value; which in this case is gravity as we are using accelerometers. This is the random walk of the sensors; the result of small errors in measurement and electronic errors. Angular random walk, for gyroscopes, is measured in $deg/\sqrt{hr}$, and velocity random walk, for accelerometers, us measured in $m/s/\sqrt{hr}$ the value denote a maximum threshold the manufacturer guarantees. A lower value is better.

Linearity error

Both sensors measurements suffers from non-linearity over the sensor range. As the measured signal changes, the output from the sensor is expected to be linear. However the signal will vary, as seen in Appendix C for the accelerometer used. It is possible to calibrate the sensors and limit the non-linearity. No such calibration has been done during this thesis, as the sensors are used in such a limited part of the sensor range that measurement linearity can be guaranteed.

Scale factor error

Both sensors are affected by scale factor errors, which can be thought of as a scaling error between the measured signal and the output signal. The expectation of a sensor would be that the measured signal and the output is scaled one to one, deviation from this relation is referred to as scale factor error [Naser and Ahmed, 2020]. Scale factor error has been limited in this thesis by the use of calibration.

Shock and vibration sensitivity

The accelerometers are affected by shock and vibration, as the accelerometers used are constructed as a suspended mass, whose displacement is measured. The shock or vibration can either force the mass in a direction or to start oscillating. This can cause the sensor to saturate or give inaccurate readings, and some time will have to pass before accurate readings can be taken again. Shock and vibration sensitivity is a factor for sensor selection rather than calibration.

Magnetism

The gyroscopes are affected by magnetism. An error which cannot be calibrated, but instead the sensors need to be shielded from the magnetic source [Dengwei et al., 2013]. During this thesis, there has been no shielding against magnetism as the mounting solution does not contain magnetic shielding.

Temperature sensitivity

Both types of sensors are affected by temperature. The temperature effects can be limited by calibration performed over a temperature range. The effect is a shift of the expected sensor value in the same manner as the bias offset, noise, and scale factor but the shift changes based on sensor temperature rather than some other source. These effects from temperature changes can be measured with a temperature chamber; by mounting the sensor package inside a temperature chamber and measuring sensor output across the intended operational temperature range.

Cross-axis

Cross-axis errors are dependent on the mounting of the sensors in the IMU as well as imperfections in the sensor. If the measured axes are not perfectly orthogonal to each other a measurement in one axis will give output on another axis as well. This is known as cross-axis error. By performing a motion along one axis and reading the sensor data of all sensors at the same time, and then comparing it to the expected values. It is possible to negate the effects of imperfect mounting.

During this thesis there was cross-axis calibration performed for the accelerometers, but not the gyroscopes. The gyroscopes were not calibrated for cross-axis error as a time saving measure.

Angular, velocity and positional drift

The IMU will drift over time, both as a result of sensor errors but also because of numerical errors from the integration of the sensor data and rounding errors within the navigational algorithm. If the sensor data is assumed to be perfect, the largest error source for the IMU will stem from integration error, as the error will accumulate over time. For angle and velocity the error will grow linearly with time and for position the error will grow with time squared, since the signals are integrated over time.

Misalignment

The IMU is also affected by the accuracy of the alignment process at startup. Alignment should inform the IMU of the orientation and position of the system in relation to the world. If the IMU is aligned incorrectly as startup the assumed values to compensate for Earth's gravity and rotation will instead accumulate as an error. For example, if the unit is supposed to start with its' z-axis measuring the gravity, the navigational algorithm will calculate a value to be used for gravity compensation during alignment. Then if the unit is started on its' side, with the z-axis perpendicular to the gravitational vector and with the x-axis sensing gravity, the calculated gravity compensation will act as a error for the z-axis as it tries to compensate for the gravity which is now sensed along the x-axis. As a result the IMU will drift along both the z-axis and the x-axis, with the calculated gravity during alignment and the actual alignment respectively. It is therefore vital that the alignment is performed correctly and that the system is placed correctly during the alignment process.

6

Calibration

This chapter details the calibrations that have been performed.
To begin with the accelerometers were measured, and the measured data was plotted as an Allan variation to determine the bias offset and velocity random walk. This measurement was only performed for the accelerometers, to verify that they were in working condition and following the manufacturers specification. The measurement is performed over a long time period while held still, then a cumulative average is made over the collected sensor data. The cumulative average can then be plotted as what is known as an Allan variance [Jurado et al., 2019].

The plots seen below in Figure 6.1, 6.2, and 6.3 are the measured values of the Accelerometers and their corresponding Allan variance plots. For each figure there are four plots for the same sensor measurement; the plots are as follows for each figure. The first graph details the raw sensor data in blue, and the same data passed through a 3rd degree butterworth low-pass filter. The filtered data is illustrated in orange. These colors will be used in the same way for all these graphs, with blue for the raw data and orange for the filtered data. The second graph is the Allan variance of the measurement data. It is worth noting that the filtering does not change the characteristics in terms of the errors for any of the sensors. The third graph presents the power spectrum of both the raw data and the filtered data. The fourth graph is the raw and filtered data presented as a moving average. This graph clearly illustrates the bias instability of the sensor, as the moving average is large enough to filter any high frequency noise of the signal.

Figure 6.2 stands out as the spectral analysis differs from Figure 6.1 and 6.3. The reason for this difference can be seen in the topmost graph in Figure 6.2, the raw data, illustrated in blue contain some other variation than just the sensor noise. A probable cause is that the sensors has experienced vibrations during the measurement period, which disrupts the measurement. As a time saving measure during the thesis, the sensor has been assumed to behave correctly and that the measurement has been disurbed by some outside factor.

No Allan variance were performed for the gyroscopes, as they are produced by Saab and have their functionality and performance verified as part of production.

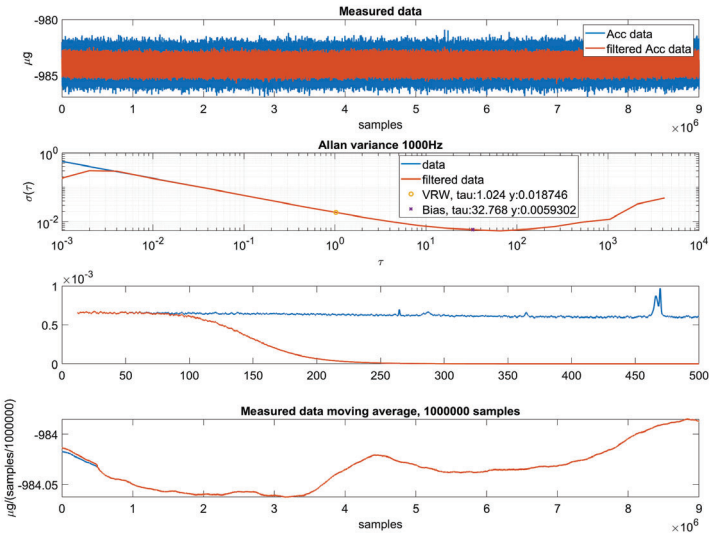

Figure 6.1 Measurement of accelerometer A1 while stationary. The topmost graph is the raw data, in blue, as well as the same data, but filtered with 3rd degree butter-worth filter, illustrated in orange. The second graph is the corresponding Allan variance for the collected data. The third graph is the power spectrum of each signal. The bottom graph is the the plot of a moving average over 1000000 samples of both the raw data and the filtered data.

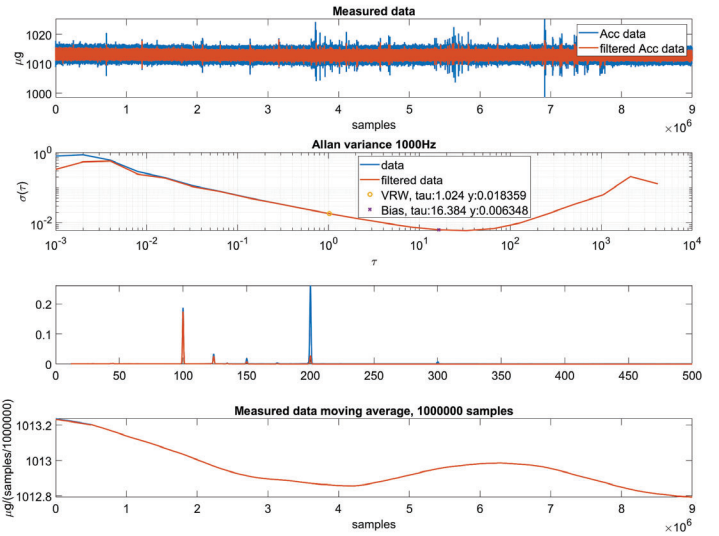

Figure 6.2 Measurement of accelerometer A2 while stationary. The topmost graph is the raw data, in blue, as well as the same data, but filtered with 3rd degree butter-worth filter, illustrated in orange. The second graph is the corresponding Allan variance for the collected data. The third graph is the power spectrum of each signal. The bottom graph is the the the plot of a moving average over 1000000 samples of both the raw data and the filtered data. The power spectrum for the measured signal show that the measurement has been disturbed by some outside force, the measurement should be redone so that the data could be trusted. The measurement has not been redone as a time saving measure.

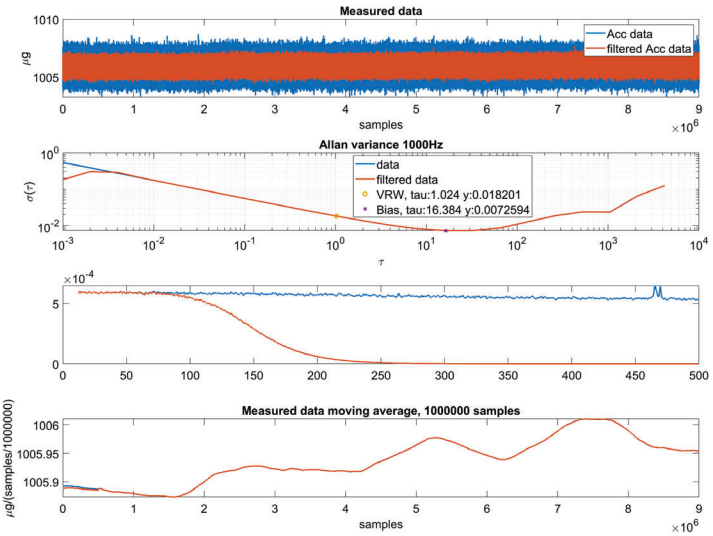

Figure 6.3 Measurement of accelerometer A3 while stationary. The topmost graph is the raw data, in blue, as well as the same data, but filtered with 3rd degree butter-worth filter, illustrated in orange. The second graph is the corresponding Allan variance for the collected data. The third graph is the power spectrum of each signal. The bottom graph is the the plot of a moving average over 1000000 samples of both the raw data and the filtered data.

6.1 Sensor calibration

Calibration of the sensors were performed on a rotation table in a temperature controlled environment. The IMU was mounted to the rotating table which is set to spin clockwise and counter-clockwise at a specific rate with periods of standstill in between the rotations. During the repetition of standstill and rotations, a temperature sweep is performed over the intended working temperature range of the sensors. The gyroscopes are operable over a range of -40 to 70 degrees Celsius, and the accelerometers are operable in the range of -40 to 125 degrees Celsius. For this thesis a smaller range of -10 degrees Celsius to 50 degrees Celsius has been used for calibration. The smaller temperature range has been used since the unit is not enclosed correctly, as it is a prototype, and therefore susceptible to condensation, another reason was to decrease the time needed for calibration.

The INS measure all the sensors during both standstill and rotations, and outputs the values to be used for calibration.

For the accelerometers, the scale factor error is calculated as the deviation from the actual measurement by measuring the absolute sensor value between the positive and the negative orientation. The measured values might not be taken at the exact same temperature, and therefore each set of measured values is used to construct a fifth order polynomial. The average of the two polynomials are then used to estimate a scale factor compensation for the sensor. The results from the measurement of the scale factors of the accelerometers can be seen below in Figure 6.4, 6.5, and 6.6.

The bias offset for the accelerometers is calculated as the average between the measured gravity in the positive orientation and the negative orientation. One orientation measuring gravity with a positive sign and the other orientation with a negative sign. The result should be zero, if there is no bias offset for the sensor. The plots of the bias error can be seen below in Figure 6.7, 6.8, and 6.9. The following graphs in Figure 6.10, 6.12, and 6.14 illustrate the correction for the scale factor and Figure 6.11, 6.13, and 6.15 the bias correction as a graph.

For gyroscopes the scale factor is calculated as the difference in the measured value between a positive rotation and a negative rotation, divided by the difference in angular velocity for the rotations, for a single axis, which should be one as the sensor should be equally sensitive for a clockwise and counter-clockwise rotation. The scale factor error is then calculated the deviation from one as a percentage. The results from the measurement of the scale factors of the gyroscopes can be seen in below in Figure 6.16, 6.17, and 6.18.

The bias is calculated as the average between two values at standstill for the gyroscopes, both before and after a clockwise rotation as well as before and after a counter-clockwise rotation. The bias error when mounted in a positive orientation can been seen in Figures 6.19, 6.21, and 6.23. The bias error when the gyroscopes are mounted in a negative orientation can be seen in 6.20, 6.22, and 6.24. One can then utilize the scale factor to convert the sensor data into drift; expressed in degrees per hour. As seen in the graphs for scale factor and bias for the gyroscopes, the values are not within the manufacturer specification. The reason is that the standard calibration made by Saab have not yet been performed for these sensors. But, with the calibration done during this thesis the sensors will be well within the specification.

Based on the scale factor error for the gyroscopes, three compensation polynomials have been calculated for each sensor as seen in Figure 6.25,6.28, and 6.31. The gyroscopes were measured in both orientations; Figures 6.26, 6.29, and 6.32 illustrate the bias compensation in the positive orientation. Fig-

ures 6.27, 6.30, and 6.33 illustrate the bias compensation factor in the negative orientation. The orange section of the graph is the intended usable temperature range for the prototype as mentioned above. The scale factor of a gyroscope does not differ depending on the orientation of the sensor, therefore only one plot is drawn of the scale factor correction polynomial. For the gyroscope bias some additional complexity is introduced as the sensor experiences more or less drift depending on the orientation. As such, the actual compensation polynomial is calculated as the average between the bias polynomial for the positive orientation of the measured axis and the bias polynomial for the negative orientation of the measured axis.

For both the accelerometers and the gyroscopes the values of the scale factor compensation and the bias offset compensation is input as compensation tables into the INS. Then for each sensor value to be compensated the INS reads the temperature of the same sensor to determine which compensation value should be used to compensate the signal. The formula for the compensation is as follows.

$$S_c = (S_r - B(t)) * SF(t) \tag{6.1}$$

where
S_r = The raw sensor value as read from the AD converter.
S_c = The compensated sensor value.
$B(t)$ = The bias compensation value at temperature t.
$SF(t)$ = The scale factor compensation value at temperature t.

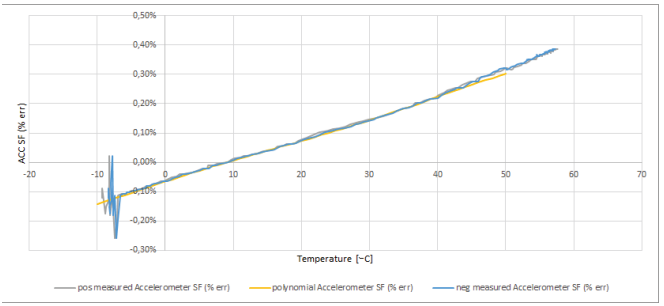

Figure 6.4 Scale factor for accelerometer 1. The Accelerometer has been measured twice, once in a positive orientation and once in a negative orientation.
The average of the two measurements are then plotted as a fifth order polynomial.

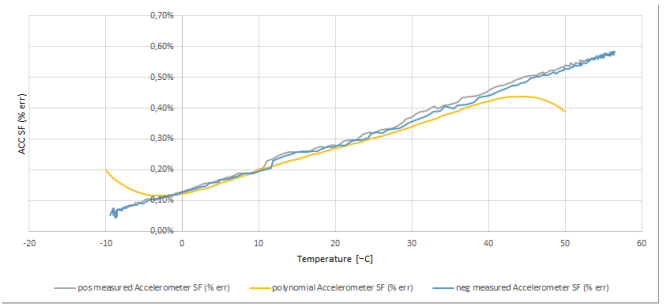

Figure 6.5 Scale factor for accelerometer 2. The Accelerometer has been measured twice, once in a positive orientation and once in a negative orientation.
The average of the two measurements are then plotted as a fifth order polynomial.

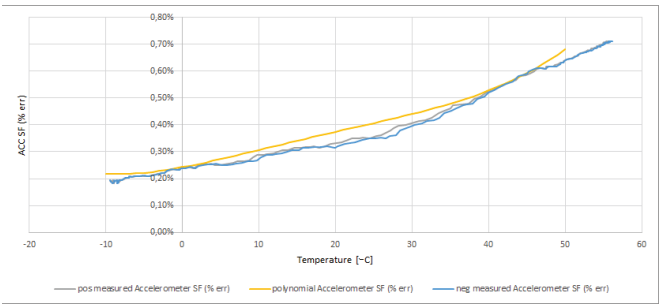

Figure 6.6 Scale factor for accelerometer 3. The Accelerometer has been measured twice, once in a positive orientation and once in a negative orientation.
The average of the two measurements are then plotted as a fifth order polynomial.

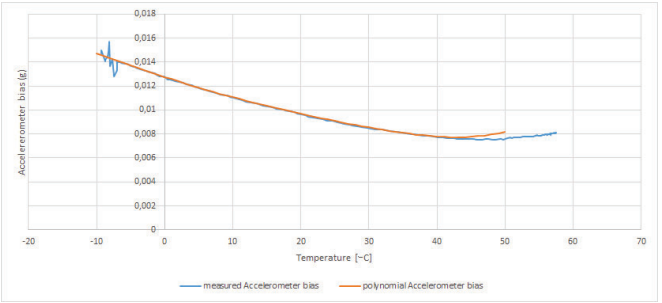

Figure 6.7 Bias for accelerometer 1.
The bias is calculated as the average between the positive measurement and the negative measurement. The polynomial is of fifth order.

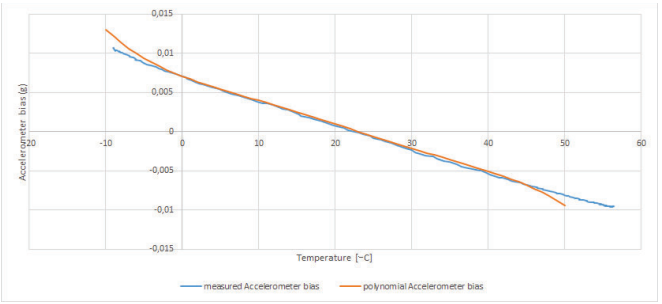

Figure 6.8 Bias for accelerometer 2.
The bias is calculated as the average between the positive measurement and the negative measurement. The polynomial is of fifth order.

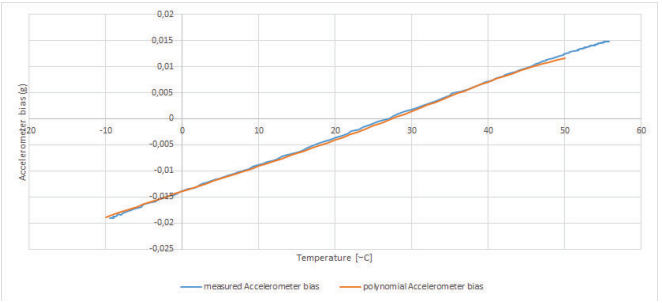

Figure 6.9 Bias for accelerometer 3.
The bias is calculated as the average between the positive measurement and the negative measurement. The polynomial is of fifth order.

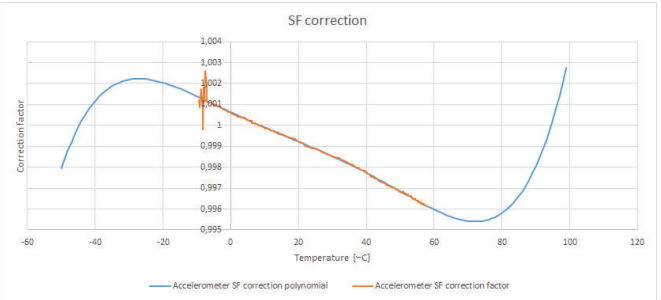

Figure 6.10 Scale factor correction for accelerometer 1

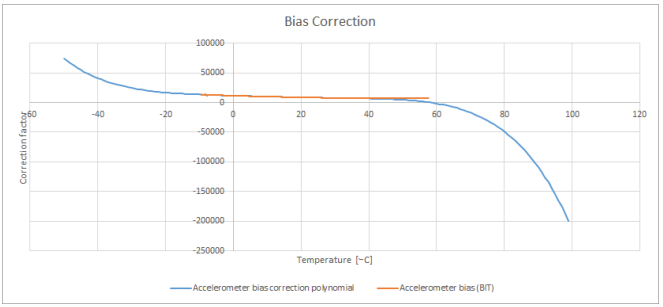

Figure 6.11 Bias correction for accelerometer 1

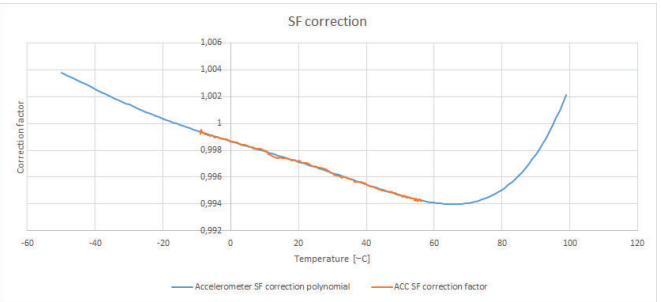

Figure 6.12 Scale factor correction for accelerometer 2

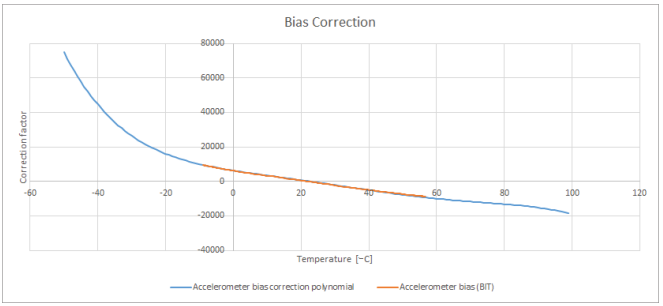

Figure 6.13 Bias correction for accelerometer 2

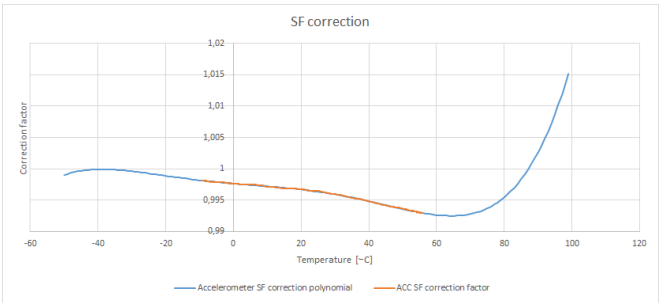

Figure 6.14 Scale factor correction for accelerometer 3

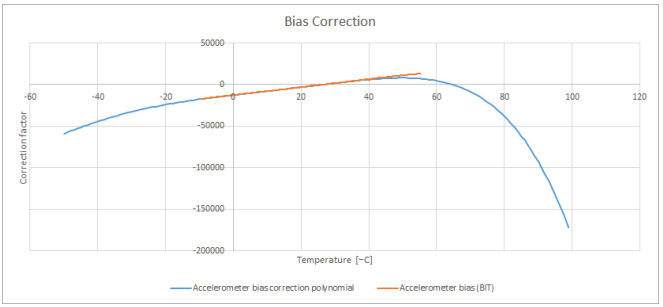

Figure 6.15 Bias correction for accelerometer 3

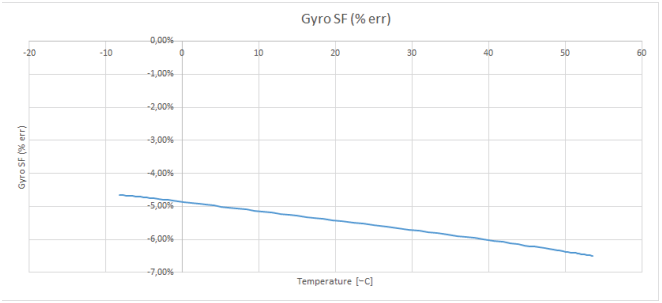

Figure 6.16 Scale factor for gyroscope 1

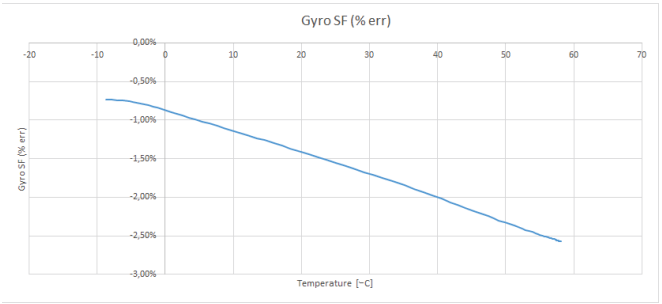

Figure 6.17 Scale factor for gyroscope 2

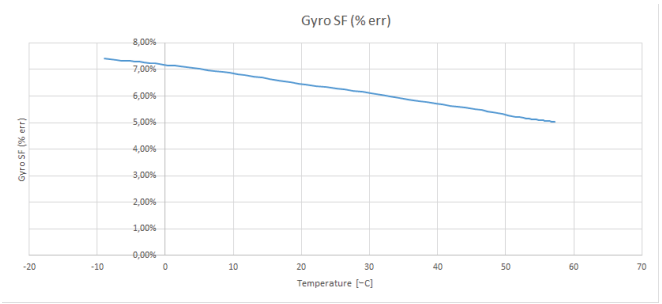

Figure 6.18 Scale factor for gyroscope 3

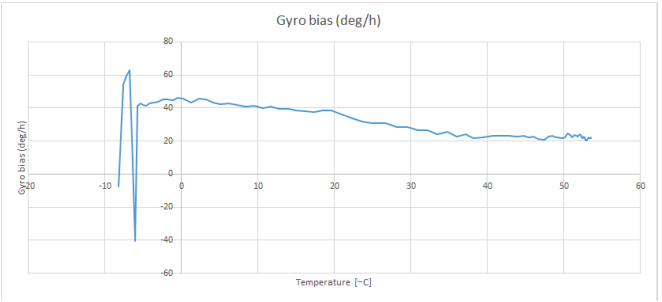

Figure 6.19 Bias for gyroscope 1 mounted in positive orientation

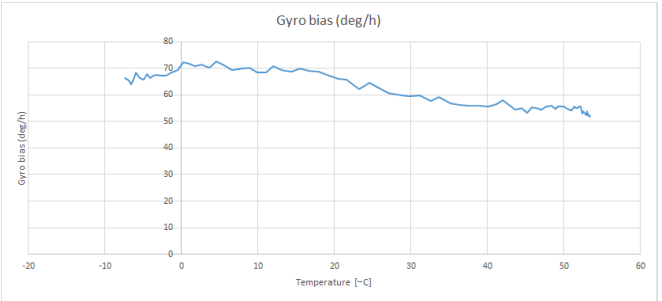

Figure 6.20 Bias for gyroscope 1 mounted in negative orientation

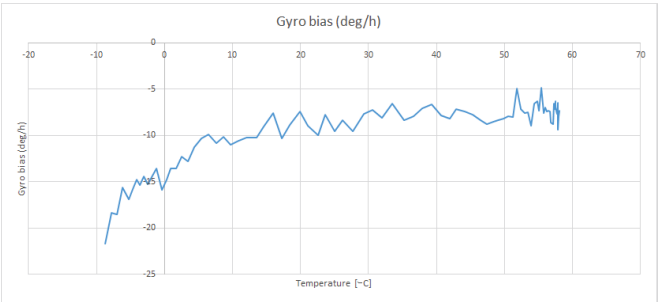

Figure 6.21 Bias for gyroscope 2 mounted in positive orientation

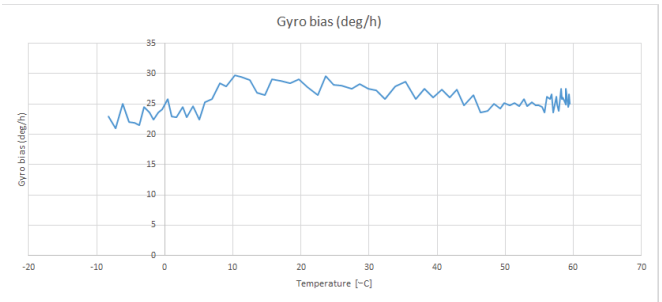

Figure 6.22 Bias for gyroscope 2 mounted in negative orientation

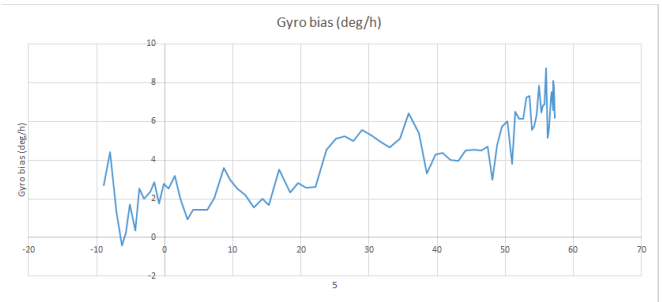

Figure 6.23 Bias for gyroscope 3 mounted in positive orientation

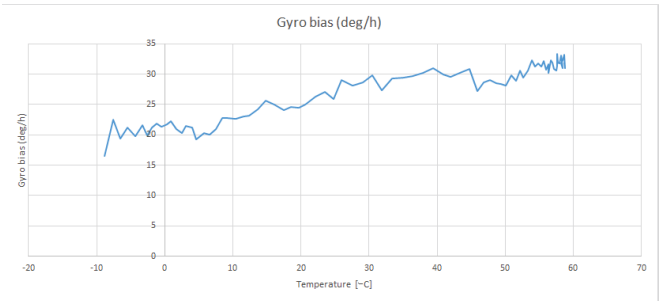

Figure 6.24 Bias for gyroscope 3 mounted in negative orientation

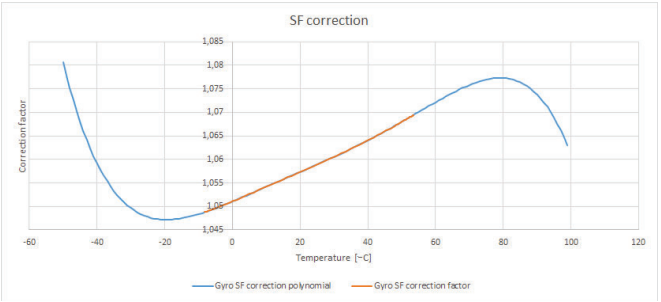

Figure 6.25 Scale factor correction for gyroscope 1

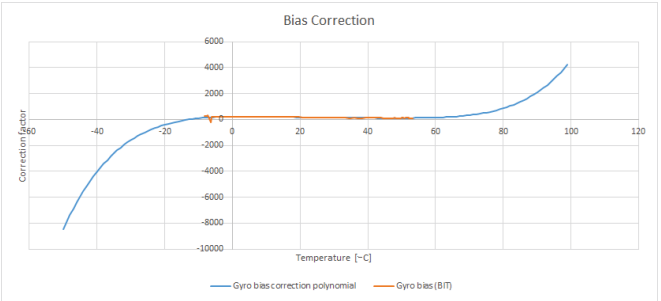

Figure 6.26 Bias correction for gyroscope 1 in positive orientation

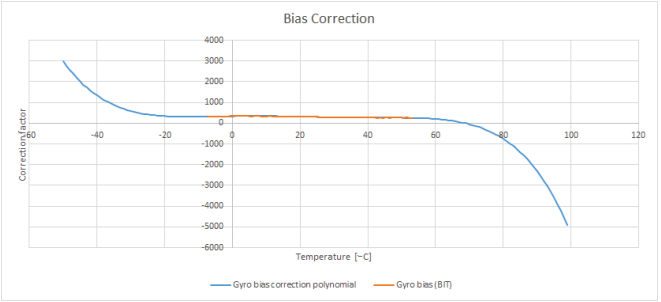

Figure 6.27 Bias correction for gyroscope 1 in negative orientation

Figure 6.28 Scale factor correction for gyroscope 2

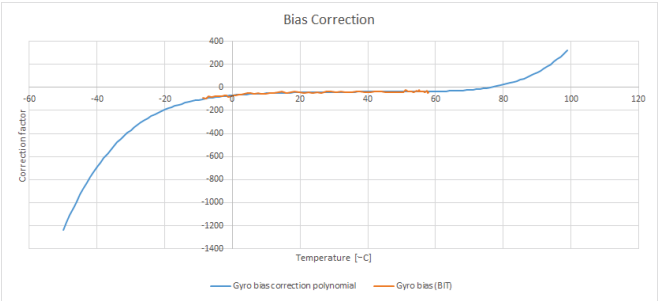

Figure 6.29 Bias correction for gyroscope 2 in positive orientation

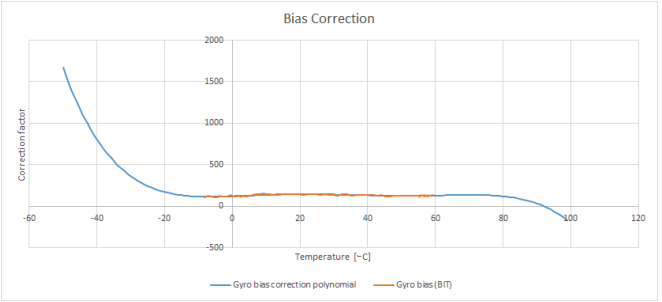

Figure 6.30 Bias correction for gyroscope 2 in negative orientation

Figure 6.31 Scale factor correction for gyroscope 3

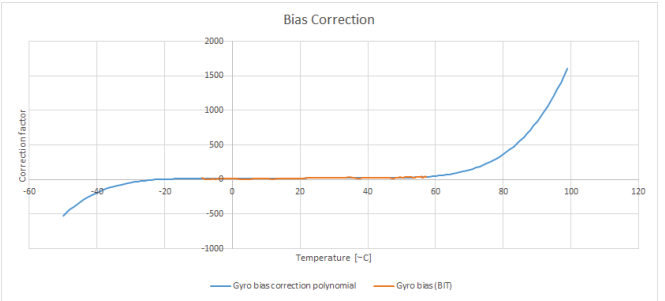

Figure 6.32 Bias correction for gyroscope 3 in positive orientation

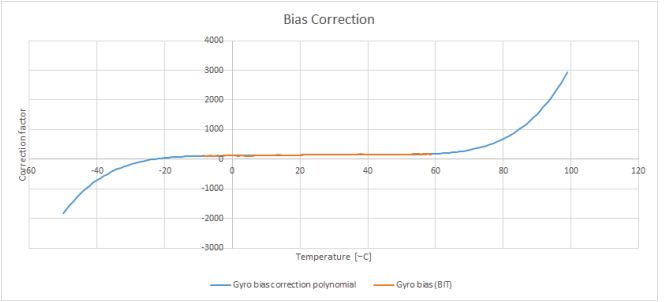

Figure 6.33 Bias correction for gyroscope 3 in negative orientation

6.2 Cross-axis

This section details the cross-axis compensation for the unit.

When mounting the accelerometers and gyroscopes, there is no guarantee of orthogonality between the sensors axes. Cross-axis error is when multiple sensors sense a change that is performed along a single axis. This is a error that can be measured and compensated for.

The cross-axis error for accelerometers is measured by placing the system on a flat surface, parallel to the Earth's surface. All sensors are read during a short period of time. The measurement process is then repeated for each axis, both in a positive and negative orientation in relation to Earth, corresponding to six measurements.

The cross-axis error is calculated as follows for a single sensor. The average of all sensor is calculated for both the measurement of the current axis in a positive orientation and a negative orientation. If no cross-axis error is present the measured axis should output the local gravity and the other two accelerometers should output 0. The deviation from the supposed value of each sensor is calculated based on the averages. Then the cross-axis compensation is calculated as a ration between the measured axis and the axis which should equal zero. For the purpose of illustration the x-axis has been used in the formulas below, but the compensation is mathematically equivalent for all axes.

$$\delta_y^x = \frac{A_x}{A_y} \tag{6.2}$$

where
A_x = The measured value in the axis not measured, should be equal to zero.
A_x = The measured value in the axis currently measured, should be equal to the local gravity.
δ_y^x = The compensation factor for the x-axis, based on the signal value measured in the y-axis.

The cross-axis compensation for the sensor mounted in the x-axis is programmed into the navigation system as follows.

$$A_{cx} = A_{rx} - A_{ry} * \delta_y^x - A_{rx} * \delta_z^x \tag{6.3}$$

where
A_{cx} = Compensated sensor value for accelerometer mounted along x-axis.
A_{rx} = Raw sensor value for accelerometer mounted along x-axis.
A_{ry} = Raw sensor value for accelerometer mounted along y-axis.
A_{rz} = Raw sensor value for accelerometer mounted along z-axis.
δ_y^x = the compensation factor for the x-axis, based on the signal value measured in the y-axis.
δ_z^x = the compensation factor for the x-axis, based on the signal value measured in the z-axis.

7

Alignment

At startup the INS needs to determine its position in relation to the center of Earth, this step is called alignment. Alignment is done by running the INS whilst the craft is stationary, this allows the sensors to measure the current attitude of the system. One could also utilize the gyroscopes to measure Earth's rotation and determine latitude for the unit.

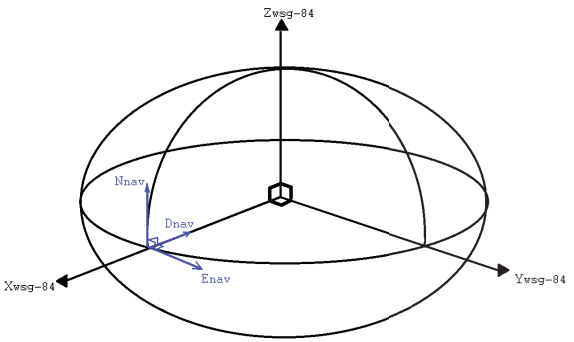

Figure 7.1 Relation between Earth and navigation frame. The navigational frame is assumed to be at Null island, 0°N 0°E. The oblateness of the Earth is exaggerated.

To begin with the transformation matrix between the navigation frame and the Earth frame is determined at startup of the craft. The navigational frame is placed with two axes, x and y, parallel to Earths surface, and with the z-axis downward to the Earths center at the local position. This constructs a navigation frame that is commonly referred to as a NED frame; a North, East, Downward frame. Assuming that the craft is started at null island, with latitude 0° and longitude 0° the frame relationship can be seen in Figure 7.1.

Based on Figure 7.1, with the craft at Earth's meridian and the Greenwich line, the following trans-

formation matrix can be constructed.

$$\begin{bmatrix} X_{Earth} \\ Y_{Earth} \\ Z_{Earth} \end{bmatrix} = \begin{bmatrix} 0 & 0 & -1 \\ 0 & 1 & 0 \\ 1 & 0 & 0 \end{bmatrix} \begin{bmatrix} N_{nav} \\ E_{nav} \\ D_{nav} \end{bmatrix} \tag{7.1}$$

However, the transformation matrix, C_N^E, will change as the position on Earth changes and can be calculated as follows.

$$C_N^E = \begin{bmatrix} -\sin(latitude)\cdot\cos(longitude) & -\sin(longitude) & -\cos(latitude)\cdot\cos(longitude) \\ -\sin(latitude)\cdot\sin(longitude) & \cos(longitude) & -\cos(latitude)\cdot\sin(longitude) \\ \cos(latitude) & 0 & -\sin(latitude) \end{bmatrix} \tag{7.2}$$

This matrix is calculated during startup with the values, for longitude and latitude, input by the user of the system.

The navigational frame also needs to utilize some mechanization so that the craft can determine the heading in reference to Earth during runtime. Either a geographically slaved azimuth, a free azimuth or a wander azimuth can be used, which now will be explained. For a geographically slaved azimuth the local frame is locked in orientation so that the horizontal axes point towards geological north and east. A simple model, however with a definitive drawback, the navigation system becomes unfit for navigation across the poles of the Earth. The drawback can be illustrated by asking a simple question; in what direction should the craft be oriented to to point north when at the north pole? In that instance, all directions traveled lead south, and the geographically slaved azimuth is undefined. A free azimuth on the other hand, references the navigation frame to inertial space, and the divergence from the geographical poles needs to be continuously calculated. The wander azimuth mechanization is a fusion between these the free and geographically slaved models. The navigation frame is horizontal to Earths surface and the azimuth angle wanders free when the vehicle is in motion, but still when the craft is stationary. Meaning that the north axis of the navigational frame drifts from the true north as the craft moves. The angle between the true north and the north of the navigation frame is called azimuth angle. However, the azimuth angle still needs to be calculated in relation to geographical north [Savage, 1997]. For this thesis, a wander azimuth has been used.

The transformation matrix between the body frame and the navigation frame determine the heading of the system as well as any attitude changes. Determining the starting attitude is vital for decreasing errors during runtime. If the system is assumed to be in one orientation but starts in another there will be drift introduced, as the system incorrectly compensates for gravity. In an extreme case the system can be assumed to be rotated 90° along a single axis, then the system assumes gravity compensation along one axis but measures gravity along another axis, introducing drift in the magnitude of $9.8 m/s^2$ in two directions.

Therefore, it is assumed that the system always start as illustrated in Figure 7.2. This simplifies the alignment process to only determining the gravity vector, as measured in X_{body}, and Y_{body} and Z_{body} is assumed to be aligned to the north and east of the navigational frame, and should therefore measure zero during alignment. The implication of the simplified alignment process is that the system always has to be started with one axis as close to parallel to the gravity vector as possible, and the other two axes has to be aligned with north and east of the navigational frame; which coincides with the north and east of the Earth at the local position at startup. Before each alignment the unit has been placed on a flat, still surface, and the rotated to align with the east and north axis of the navigational frame. A analog compass has been used to determine the magnetic north of the Earth during alignment.

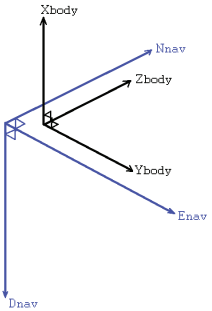

Figure 7.2 Relation between the navigation and body frame.

The transformation matrix between navigation and body frame, C_B^N, is defined during alignment, but based on how the axes are oriented in Figure 7.2 the following matrix can be used for illustration purposes. The representation that follows will be essentially the same as the matrix produced during alignment, any difference introduced that skews the matrix from the example in this report is based on the system not being placed completely flat against the surface of the Earth.

$$\begin{bmatrix} N_{nav} \\ E_{nav} \\ D_{nav} \end{bmatrix} = \begin{bmatrix} 0 & 0 & 1 \\ 0 & 1 & 0 \\ -1 & 0 & 0 \end{bmatrix} \begin{bmatrix} X_{body} \\ Y_{body} \\ Z_{body} \end{bmatrix} \tag{7.3}$$

The matrix is calculated as follows during alignment. First, an average of the accelerometers are taken, which is then divided by the approximated gravity based on the units position, and stored in the third row of the C_B^N matrix.

The second row of the C_B^N matrix is then assumed to be

$$C_{21} = -C_{32} \tag{7.4}$$
$$C_{22} = 0 \tag{7.5}$$
$$C_{23} = C_{31} \tag{7.6}$$

The first row of C_B^N is calculated as the cross-product of the second and third row, as:

$$C_{11} = C_{22}C_{33} - C_{23}C_{32} \tag{7.7}$$
$$C_{12} = C_{23}C_{31} - C_{21}C_{33} \tag{7.8}$$
$$C_{13} = C_{21}C_{32} - C_{22}C_{31} \tag{7.9}$$
$$\tag{7.10}$$

Thus, alignment is finished and the system is ready to run.

8

Software

The software is implemented for the particular processor used in C, using the same software that Saab use for interfacing the gyroscopes for stabilization purposes. This allows for standardization on the interfacing with the gyroscopes and accelerometers, and more time during this thesis can be spent on the navigation algorithm. The software also has to be modified to send out navigational data. The software is intended to be as modular as possible to allow for future modifications and re-use, introducing little or no changes to existing code if possible.

8.1 Software overview

The AD converter reads the analog signals from the sensors and converts the signal to digital data, which is sent over a serial interface to the processor board. The AD converts the values from each of the sensors sequentially and converts the analog signal to a digital equivalent. The ADC samples each sensor at a rate of approximately $7000Hz$. The processor receives interrupts for each new value sent over the serial interface. The interrupt trigger the separate calculation processor which adjust the measured data using the temperature for the relevant sensor as well as calculating an average of 7 values, bringing the rate down to approximately $1000HZ$ for each sensor. This allows for slower processing of the measured values in the navigational algorithm. The use of the calculation processor offloads the signal processing and error compensation computations from the CPU, freeing up capacity for the navigation algorithm and communication.

The average of the sensor data is sent to the main CPU as an interrupt. The CPU interrupt scales the values from a voltage level into either angular rate or acceleration. The CPU interrupt calculates an integral over the latest four values for each sensor, getting change in angle and velocity for the system during a two samples in time. The integral is then buffered by the CPU.

The buffered values are then further processed as part of a function, a generic task, which the processor runs at a set pace as part of the main loop. The buffer allows for the CPU interrupt to write values continuously without interfering with the accessing of the values for the navigation algorithm as long as the generic task is run at a high enough pace.

The navigation algorithm has been implemented as part of the generic task function call. The generic task also prints the navigation data at a set pace, slower than that of the navigational algorithm.

The data flow within the system can be seen below in Figure 8.1. The figure is an abstraction as it contains both hardware components, the sensors and the AD converter. As well as software components, such as the CPU interrupt and main process.

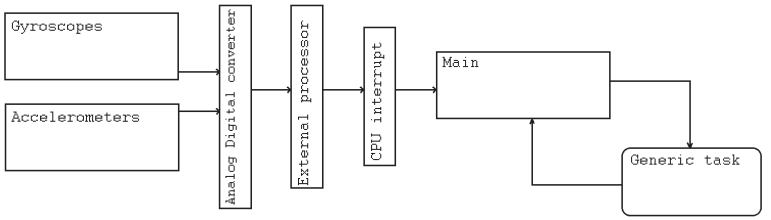

Figure 8.1 Software overview and data flow from sensors. An abstraction showing how different parts of the system interconnect.

8.2 Software implementation

The navigational algorithm has been implemented as the analytically exact solution as defined in Appendix A. Note that Equation A.12 has been revised to $C_{N_{I(m-1)}}^{N_{I(m)}} = I + f_1(\zeta_m)(\underline{\zeta}_m\times) + f_2(\zeta_m)(\underline{\zeta}_m\times)^2$ according to Strapdown Inertial Navigation Technology, second edition [Titterton D. H., 2004]. As the officially published version from Savage contain a typo.

As the intent of the prototype is to test the computational capacity of the processor and the fiber optical gyroscopes as components in a inertial navigation system; there is no need or possibility to do dynamic changes in the system. Therefore, all signals have been integrated with a simple trapezoidal integral and no additional compensation has been performed for dynamic motions as specified by Savage [Savage, 2015].

There are proposals for separation of the navigational algorithm by Savage, and Titteron and Weston to limit the computational load. The separation is possible since even for a system that changes dynamically, effects from the Earth does not change faster [Savage, 2015] [Titterton D. H., 2004]. No such separation has been performed during the implementation of the navigational algorithm during this thesis. Doing so would decrease the computational load but increase development time; which is why it was avoided. Additionally, the system has been implemented with a wander azimuth as specified in Chapter 7, which sets $\rho_{ZN} = 0$. Which in turn simplifies Formula A.24 to

$$\underline{\xi}_m \approx (3F_{C_{m-1}}^N - F_{C_{m-2}}^N)(\underline{u}_{Up}^N \times \Delta\underline{R}_m^N)] \tag{8.1}$$

The alignment process has been implemented as a simplified version of the alignment proposed by Savage, for example there has been no gyrocompassing implemented [Savage, 1997].

9

Results

As seen in Section 6.1, the offset and scale factor error graphs of the accelerometers are well within the margin specified by the specifications as seen in Appendix C. The gyroscopes were not within the specification provided as they were not calibrated. However, the introduction of the calibration tables does bring the sensors well within the specification. As such; any error source larger than the specification for the accelerometers and gyroscopes is introduced either by the navigational algorithm or as rounding errors.

The timing of the navigational algorithm has been verified with an oscilloscope. The processor was programmed to pull a pin high during the duration of the CPU interrupt responsible for the integration of the signal data, as well as pulling a pin high during the time from the start of the processing of data for the navigation algorithm until the process output navigational data. Measuring the pins when the INS is running verify that there is additional time for the navigational algorithm to be run when performing the trapezoidal integral as it is currently done.

It is not possible to increase the rate of the integration without optimization of the navigation algorithm as the rate at which the navigation algorithm can be run was to slow. Thus it has been determined that it is possible to build a functional INS with the current hardware that Saab uses, and as such **RQ1** has been answered. As it stands the INS can determine the attitude of the system accurately during a short standstill test as seen in Figure 9.1. However, the system drifts as a result of some numerical error in the calculation of the velocity and position of the unit as seen in Figures 9.2 and 9.3. It should be noted that the two figures are from two separate measurements.

One would expect an acceleration in one direction with a subsequently de-acceleration in the same direction would correspond to the velocity to return to zero, this is not the case currently. There is some numerical error which accumulate the acceleration and the de-acceleration instead leading to a large drift in velocity and position. This drift in velocity and position is notable during standstill testing, but even more apparent during movements. Testing of the performance of the INS was limited to standstill testing as a result of this large error in velocity and position.

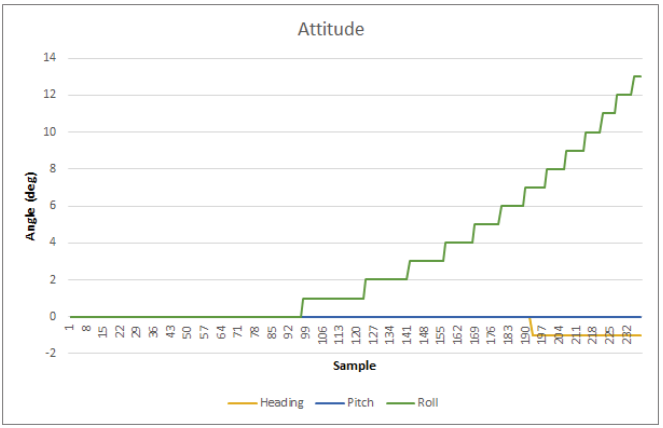

Figure 9.1 The attitude change of the prototype during a standstill test of 5 minutes.

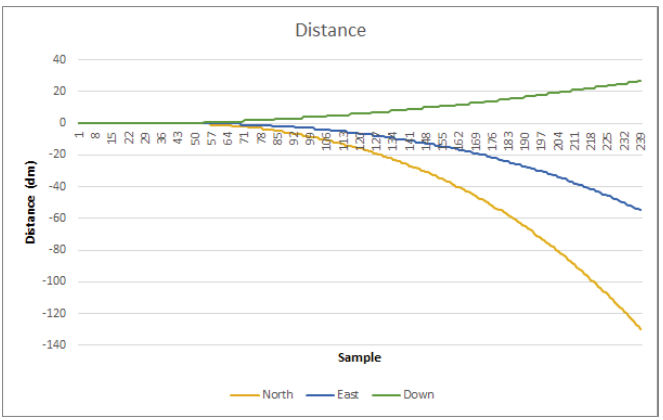

Figure 9.2 The change in position for the prototype during a standstill test of 1 minutes

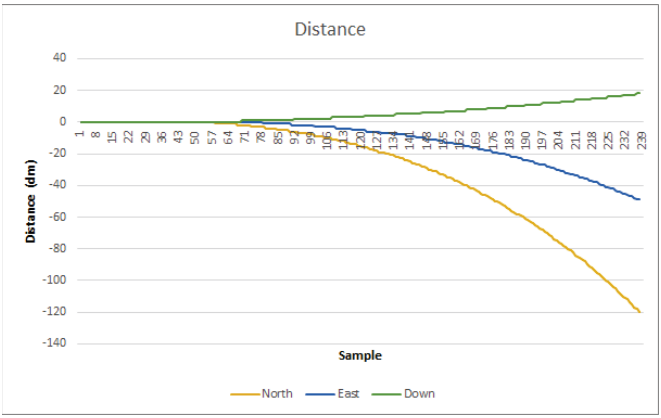

Figure 9.3 The change in position for the prototype during a standstill test of 1 minutes

10

Discussion

This chapter details any considerations and conclusions that can be made in regards to the findings presented in Chapter 9. It will also answer the goals that were posed in Section 2.1; which are repeated below.

- **RQ1**: Can existing hardware within Saab be used for navigation?
- **RQ2**: For how long is an inertial navigation system with the provided hardware trustworthy?
- **RQ3**: What, if any, changes need to be realized in hardware and software to produce a working navigation system?

As far as hardware, the hardware used during this thesis allow for navigation, there could be improvements made that would affect the system positively but which will have to be determined when the navigation algorithm is correct. The largest error source currently stems from errors with the implementation of the navigation algorithm. There could be additional improvements introduced in software, but any such optimization should be introduced when the system performs in an accurate way.

Based on the large numerical errors that remain in the navigation algorithm this thesis reaches no conclusion for **RQ2** and **RQ3**. The answers to those questions will have to be answered in some future work.

The work performed during this thesis is applicable to any hardware, and based on this report one should be able to get a base understanding of how a strapdown inertial navigation system works. The physics and the mathematical model will hold for any system, and one could use hardware and programming language to implement the navigation algorithm. But, base on this thesis being performed in conjunction with Saab many parts are also purposely obscured to protect trade secrets.

10.1 Ethical considerations

An inertial navigation system is a highly useful tool in many applications; such as aerospace, drones, robots, and unmanned vehicles. Inertial navigation system also hold an important role in military applications for missile guidance and navigation in military application when detection should be avoided; such as submarines.

The navigation system developed during this thesis has no use as a standalone product, but might be incorporated into either civilian or military applications later.

As such, each individual should consider their technological contribution to society as well as how accessible they make the technology produced. In this case, there is no determined use case yet, but rather the use will be determined later on. Therefore an ongoing discussion will have to be held in relation to who receive access to the finding and results, and any product that might stem from those findings.

In the same manner is it of great importance that technology with dual-use is regulated, and controlled so that access is only granted in the correct setting. Any one who contribute to advances within dual-use technology, should also partake in the discourse on the uses of the same technology; this avoids separation between those who develop the technology and those who regulate the uses of the technology. This cooperation will be beneficial to a more accurate cost-benefit analysis, as any technology can be used in multiple settings and the contribution to society might outweigh the negative impact the technology might bring when used in the wrong setting.

10.2 Future work

The findings of this thesis, leaves inconclusive results regarding the performance of the navigational system. Clearly, the first order of action is to eliminate the drift in velocity and position as that is the largest error source of the system. Additionally, there are several important fields where there could be additional implementations and testing can be performed. Below are some of the areas that have been identified for future development.

As written in [Savage, 1997], the transformation matrices should be run through an orthonormalization algorithm. No such method has been implemented during this thesis. The implementation and testing of such an algorithm is interesting in both the aspect of timing and improved accuracy and is a definitive path forward when developing the prototype further.

A interesting area of development would also be improvement in the mounting solution, with a construction which centers the sensors in respect to each other. Additionally an improved alignment algorithm, rather than the bare minimum which is implemented now should improve the performance.

There is also areas where the prototype can be improved which has not been researched during this thesis. For example there has been no filtering of the signals performed. Kalman filtering is an important field of research within inertial navigation and when the system is operational there might be additional performance to be gained by signal filtering. Any filters introduced will have to be tested to verify any improvement in performance.

The ADC used only allows the system to sequentially sample the sensors, as specified in Chapter 8.1. Whilst there has been no noticeable error for this, it would be interesting to compare it the accuracy of a system which samples the sensors simultaneously. This would take a considerable amount of work to implement and test, as the two system should be computationally equivalent to be comparable, but is nevertheless interesting.

In short, there remains many areas of improvement for this prototype. Especially to bring the prototype to a finished product; but many still just to get the best performance possible out from the prototype.

A

P.G Savage model

The following descriptions have been used for the navigational system. The model used in this paper has been defined by Paul G. Savage and is copied below for reader convenience [Savage, 2015].

B frame = "Body", coordinate frame parallel to strapdown inertial sensor axes.

N frame = "Navigation", coordinate frame having the Z axis parallel to the upward vertical at the local position location. A "wander azimuth" N Frame has the horizontal X, Y axes rotating relative to the non-rotating inertial space at the local vertical component of Earth's rate about the Z axis. A "free azimuth" N Frame would have zero inertial rotational rate of X, Y axes around the Z axis. A "geographic" N Frame would have the X, Y axes rotated around Z to maintain the Y axis parallel to the local true north.

E Frame = "Earth" referenced coordinate frame with fixed angular geometry relative to the rotating earth.

I Frame = "Inertial" non-rotating coordinate frame.

A,A_1,A_2,A_3 = Arbitrary coordinate frame

$\underline{V}$ = Vector without specific coordinate frame designation

$\underline{V}^A$ = Column matrix with elements equal to the projection of $\underline{V}$ on Frame A axes.

$C_{A_2}^{A_1}$ = Direction cosine matrix that transforms a vector from its Coordinate Frame A_2 projection form to its Coordinate Frame A_1 projection form.

$\underline{\omega}_{A_1A_2}$ = Angular rate of coordinate Frame A_2 relative to coordinate Frame A_1. When A_1 is the inertial I frame, $\underline{\omega}_{A_1A_2}$ is the angular rate measured by angular rate sensors mounted on Frame A_2.

$\Omega_{A_1A_2}^{A_3}$ = Skew symmetric (or cross-product) form of $\underline{\omega}_{A_1A_2}^{A_3}$ represented by the square matrix

$$\begin{bmatrix} 0 & -\omega_{Z_{12}}^3 & \omega_{Y_{12}}^3 \\ \omega_{Z_{12}}^3 & 0 & -\omega_{X_{12}}^3 \\ -\omega_{Y_{12}}^3 & \omega_{X_{12}}^3 & 0 \end{bmatrix}$$

where $\omega_{X_{12}}^3$, $\omega_{Y_{12}}^3$, $\omega_{Z_{12}}^3$ are the components of $\underline{\omega}_{A_1A_2}^{A_3}$. The matrix product of $\Omega_{A_1A_2}^{A_3}$ with another A_3 Frame vector equals the cross-product of $\underline{\omega}_{A_1A_2}^{A_3}$ with the vector in the A_3 Frame. Because $\Omega_{A_1A_2}^{A_3}$ is skew symmetric, its transpose equals its negative.

$\dot{()} = \frac{d()}{dt}$ = Derivative with respect to time

Savage then defines the following formulas which can be used to calculate the motions of the inertial navigation system.

Attitude

$$\dot{C}_B^N = C_B^N(\underline{\omega}_{IB}^B\times) - (\underline{\omega}_{IN}^N\times)C_B^N \tag{A.1}$$
$$\underline{\omega}_{IE}^N = (C_N^E)^T\,\underline{\omega}_{IE}^E \tag{A.2}$$
$$\underline{\omega}_{EN}^N \equiv \underline{\rho}^N = F_C^N(\underline{u}_{Up}^N\times\underline{v}^N) + \rho_{ZN}\underline{u}_{ZN}^N \tag{A.3}$$
$$\underline{\omega}_{IN}^N = \underline{\omega}_{IE}^N + \omega_{EN}^N \tag{A.4}$$

where

$\underline{\rho}^N$ = Conventional notation for ω_{EN}^N, also known as "transport rate", and analytically defined as the angular rate of Frame N relative to Frame E.

ρ_{ZN} = Vertical component of $\underline{\rho}^N$. For a "wander azimuth" N Frame, $\underline{\rho}^N$ is zero. For a "free azimuth" N frame, $\underline{\rho}^N$ is the downward vertical component of Earth's inertial angular rate.

F_C^N = Curvature matrix in the N Frame that is a function of position location over the earth.

$\underline{v}$ = Velocity (rate of change of position) relative to earth.

$\underline{u}_{Up}$ = Unit vector upward at the current position location (parallel to the N Frame Z axis)

Velocity

$$\underline{v}^E \equiv \dot{\underline{R}}^E \tag{A.5}$$
$$\underline{v}^N = C_E^N\underline{v}^E \tag{A.6}$$
$$\dot{\underline{v}}^N = C_B^N\underline{a}_{SF}^B + \underline{g}^N - \underline{\omega}_{IE}^N\times(\underline{\omega}_{IE}^N\times\underline{R}^N) - (\underline{\omega}_{IN}^N + \underline{\omega}_{IE}^N)\times\underline{v}^N \tag{A.7}$$

where

$\underline{R}$ = Position vector from Earth's center to the current position location.

$\underline{a}_{SF}$ = Specific force acceleration defined as the instantaneous time rate of change of velocity imparted to a body relative to the velocity it would have sustained without disturbances in local gravitational vacuum space. Sometimes defines as total velocity change rate minus gravity. Accelerometers measure $\underline{a}_{SF}$.

$\underline{g}$ = Mass attraction gravity at the current position location minus mass attraction gravity at the center of the earth. Sometimes denoted as "gravitation".

Position

$$\dot{C}_N^E = C_N^E(\underline{\rho}^N\times) \tag{A.8}$$
$$\dot{h} = \underline{u}_{Up}^N\cdot\underline{v}^N \tag{A.9}$$

From the gyroscopes and accelerometers the system reads $\underline{\omega}_{IB}^B$ and $\underline{a}_{SF}^B$ continuously.

These formulas have been adapted in software using the numerical exact derivations which can be expressed as, once again as defined by Savage. The exact integral solution for attitude, velocity and position is as follows.

Attitude

$$C_{B_m}^{N_{m-1}} = C_{B_{m-1}}^{N_{m-1}} C_{B_{I(m-1)}}^{B_{I(m-1)}} \tag{A.10}$$

$$C_{B_m}^{N_m} = C_{N_{I(m-1)}}^{N_{I(m)}} C_{B_m}^{N_{m-1}} \tag{A.11}$$

$$C_{B_{I(m-1)}}^{B_{I(m-1)}} = I + f_1(\phi_m)(\underline{\phi}_m\times) + f_2(\phi_m)(\underline{\phi}_m\times)^2 \tag{A.12}$$

$$C_{N_{I(m-1)}}^{N_{I(m)}} = I - f_1(\zeta_m)(\underline{\zeta}_m\times) + f_2(\zeta_m)(\underline{\zeta}_m\times)^2 \tag{A.13}$$

Velocity

$$\underline{v}_m^N = \underline{v}_{m-1}^N + \Delta\underline{v}_{SF_m}^N + \Delta\underline{v}_{G/COR_m}^N \tag{A.14}$$

$$\Delta\underline{v}_{G/COR_m}^N = \int_{t_{m-1}}^{t_m} \underline{\dot{v}}_{G/COR}^N dt \approx \frac{1}{2}(3\underline{\dot{v}}_{G/COR_{m-1}}^N - \underline{\dot{v}}_{G/COR_{m-2}}^N)T_m \tag{A.15}$$

$$\underline{\dot{v}}_{G/COR_m}^N \equiv \underline{g}^N - \underline{\omega}_{IE}^N \times (\underline{\omega}_{IE}^N \times \underline{R}^N) - (\underline{\omega}_{IN}^N + \underline{\omega}_{IE}^N) \times \underline{v}^N \tag{A.16}$$

$$\Delta\underline{v}_{SF_m}^N = \frac{1}{2}(C_{N_{I(m-1)}}^{N_{I(m)}} + I)\Delta\underline{v}_{SF_m}^{N_{m-1}} \approx \frac{1}{2}(2C_{N_{I(m-2)}}^{N_{I(m-1)}} - C_{N_{I(m-3)}}^{N_{I(m-2)}} + I)\Delta\underline{v}_{SF_m}^{N_{m-1}} \tag{A.17}$$

$$\Delta\underline{v}_{SF_m}^{N_{m-1}} = C_{B_{m-1}}^{N_{m-1}} \Delta\underline{v}_{SF_m}^{B_{m-1}} \tag{A.18}$$

$$\Delta\underline{v}_{SF_m}^{B_{m-1}} = \int_{t_{m-1}}^{t_m} C_{B(t)}^{B_{I(m-1)}} \underline{a}_{SF}^B = [I + f_2(\phi_m)(\underline{\phi}_m\times) + f_3(\phi_m)(\underline{\phi}_m\times)^2]\underline{\eta}_m \tag{A.19}$$

$$\tag{A.20}$$

Position

$$h_m = h_{m-1} + \Delta h_m \tag{A.21}$$

$$C_{N_{E(m)}}^E = C_{N_{E(m-1)}}^E C_{N_{E(m)}}^{N_{E(m-1)}} \tag{A.22}$$

$$C_{N_{E(m)}}^{N_{E(m-1)}} = I + f_1(\xi_m)(\underline{\xi}_m\times) + f_2(\xi_m)(\underline{\xi}_m\times)^2 \tag{A.23}$$

$$\underline{\xi}_m \approx \int_{t_{m-1}}^{t_m} \underline{\rho}^N \approx \frac{1}{2}[(3\rho_{ZN_{m-1}} - \rho_{ZN_{m-2}})\underline{u}_{Up}^N T_m + (3F_{C_{m-1}}^N - F_{C_{m-2}}^N)(\underline{u}_{Up}^N \times \Delta\underline{R}_m^N)] \tag{A.24}$$

$$\Delta h_m = \underline{u}_{Up}^N \Delta\underline{R}_m^N \tag{A.25}$$

$$\Delta\underline{R}_m^N \equiv \int_{t_{m-1}}^{t_m} \underline{v}^N dt \approx (\underline{v}_{m-1}^N + \frac{1}{2}\Delta\underline{v}_{G/COR_m}^N)T_m + \Delta\underline{R}_{SF_m}^N \tag{A.26}$$

$$\Delta\underline{R}_{SF_m}^N = \frac{1}{6}(C_{N_{m-1}}^{N_m} - I)\Delta\underline{v}_{SF_m}^{N_{m-1}} T_m + C_{B_{m-1}}^{N_{m-1}} \Delta\underline{R}_{SF_m}^{B_{m-1}} \tag{A.27}$$

$$\approx \frac{1}{6}(2C_{N_{m-2}}^{N_{m-1}} - C_{N_{m-3}}^{N_{m-2}} - I)\Delta\underline{v}_{SF_m}^{N_{m-1}} T_m + C_{B_{m-1}}^{N_{m-1}} \Delta\underline{R}_{SF_m}^{B_{m-1}} \tag{A.28}$$

$$\Delta\underline{R}_{SF_m}^{B_{m-1}} = \int_{t_{m-1}}^{t} \int_{t_{m-1}}^{\tau} C_{B_{I(\tau)}}^{B_{I(m-1)}} \underline{a}_{SF}^B d\tau_1 d\tau = [I + 2f_3(\phi_m)(\underline{\phi}_m\times) + 2f_4(\phi_m)(\underline{\phi}_m\times)^2]\underline{\kappa}_m \tag{A.29}$$

with

$$f_1(\chi) \equiv \frac{\sin\chi}{\chi} \tag{A.30}$$

$$f_2(\chi) \equiv \frac{1-\cos\chi}{\chi^2} \tag{A.31}$$

$$f_3(\chi) \equiv \frac{1}{\chi^2}\left(\frac{1-\sin\chi}{\chi^2}\right) \tag{A.32}$$

$$f_4(\chi) \equiv \frac{1}{\chi^2}\left(\frac{1}{2}-\frac{1-\cos\chi}{\chi^2}\right) \tag{A.33}$$

B

Saab 8088000-4xx gyroscope

FIBER OPTIC GYRO
8088 000-4xx DIGITAL/ANALOG

The new generation of Saab´s high performance Fiber Optic Gyro with both analog and digital output. Backed up by over 50-years' experience in inertial sensors.

This new generation Fiber Optic Gyro is specifically designed for stabilization applications where there is a need for high performance single-axis rate sensing. The units are equipped with both analog and digital interface in parallel giving the flexibility to be used as a standard configuration in various systems.

Operation:
A Fiber Optic Gyro is based on the Sagnac effect. The time for light to travel in a coil is dependent of the rotation of the coil. In a ring fiber optic gyro light is divided into two beams entering a fiber coil in opposite directions. After exiting the coil the two beams are combined in a coupler and a phase difference proportional to the rate of rotation is measured

Fiber Optic Gyro (FOG).

Applications:
- Gun stabilization
- Missile stabilization
- Inertial measurement units
- Sight stabilization
- Camera stabilization
- Antenna stabilization
- Autonomous vehicles

Features:
- Solid state
- Low drift
- High shock usability
- No delay on analog interface
- High internal sampling rate
- Low delay on digital interface
- Single +5VDC Supply
- Small size
- Available in EMI protected version

Company Background:
Saab has been a producer of gyros of various designs for over 50 years. Production was initially intended for Saab designed aircraft sight and missile requirements.

Since the end of 70´s, the gyro production have expanded into a product line of its own including design and production of gyro products for worldwide customers. Up to the present time, we have produced more than 50.000 sensors. Gyros based on FOG technology has been the main product since the end of 90´s.


Mechanical Gyros.

DIMENSIONAL DRAWING 8088 000-4xx

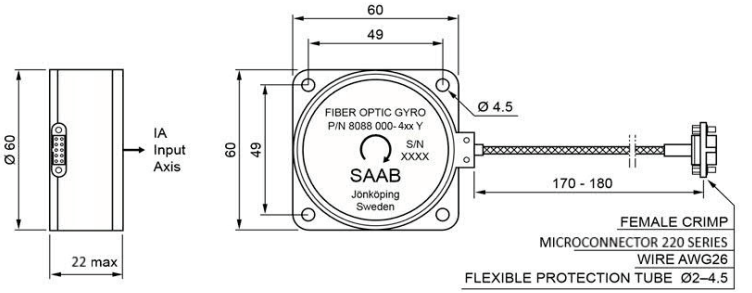

SPECIFICATION VERSION 8088 000-4xx

CHARACTERISTICS	UNIT	VALUE
Range	°/s	50 -350
Bias at 20°C (initial cond.)	°/h	20
Bias variation peak to peak over temperature range	°/h	40
Bias stability	°/h rms	1
SF error in Room Temperature	%	0.1
SF variation Over Temperature Range	%	0.3
Linearity error 0-150 °/s	% of Full Scale	0.2
Bandwidth	Hz	<1000
Start up time	msec	100
Weight	grams max	100
Temperature Sensor Output		
Built In Test Output		
POWER REQUIREMENTS		
Supply Voltage	VDC	+5 (4.90 to 5.25)
Input Power	W	1.5
ENVIRONMENTS		
Shock	g : msec	90 : 6
Vibration, sine	g : Hz	10 : 20-2000
Vibration, random	g^2/Hz : Hz	0,09 : 20-2000
Operating temperature range (OTR)	ºC	-40 to +70
Storage temperature range	ºC	-46 to +75
DIGITAL OUTPUT FORMAT RS422		
Resolution	Bits	20-24
Transmission Rate	kBaud	115.2 – 921.6
Output Update Rate	kHz	1-4
ANALOG OUTPUT FORMAT		
Differential Output	VDC	±4
Output Load	kΩ	10

Specifications subject to change without notice Sept 2020

C

Safran accelerometer

ELECTRONICS & DEFENSE

MS1000L - Datasheet

Single axis analog accelerometer

The MS1000L product is a cost-effective MEMS capacitive accelerometer based on a bulk micro-machined silicon element specifically designed for highest stability. The product is low power, fully calibrated, robust up to 6'000 g and extremely stable.

The internal electronic circuit integrates a signal conditioning with a differential analog ±2.7V output, a built in self-test and a temperature sensor available for improving accuracy by thermal compensation. The sensor is self-contained and packaged in a 20-pin LCC ceramic housing, thus insuring a full hermeticity for harsh environments.

Key features

- **Non-linearity: 0.3% FS**
- **Noise in band: 7 µg/√Hz (2g range)**
- **Excellent bias repeatability**
- **Small hermetic LCC20 ceramic package**
- **Reliable in harsh environment**
- **Single 3.3V power supply**

Key Parameters, typical values	**MS1002L**	**MS1005L**	**MS1010L**	**MS1030L**	**MS1050L**	**MS1100L**	**Unit**
Full-Scale acceleration	± 2	± 5	± 10	± 30	± 50	± 100	g
Bias temp. coefficient	± 0.1	± 0.25	± 0.5	± 1.5	± 2.5	± 5	mg/°C
Noise (in band)	7	17	34	102	170	339	µg/√Hz
In-run bias stability	3	7.5	15	45	75	150	µg
Scale Factor Sensitivity	1350	540	270	90	54	27	mV/g
Scale factor temp. coefficient	120	120	120	120	120	120	ppm/°C
Non-Linearity (IEEE Norm)	0.3	0.3	0.3	0.3	0.3	0.3	%
Axis misalignment	3	3	3	3	3	3	mrad
Power consumption	10	10	10	10	10	10	mW
Operational temperature	-40 to +125	-40 to +125	-40 to +125	-40 to +125	-40 to +125	-40 to +125	°C
Size	9 x 9	9 x 9	9 x 9	9 x 9	9 x 9	9 x 9	mm^2
Resonant frequency	1.8	3	4	6	9	14	kHz

Featured Applications (non-exhaustive):

Aerospace & Defense:
Inertial Measurement Units (IMUs)
avionics (fix wings and rotary wings): FCS, autopilot,
attitude systems (AHRS, stand by),
weapon launch systems – platform stabilization
GPS aided guidance & navigation UAV systems
short range guidance, robotics

Naval & Land:
North finding, antenna, sonar orientation
ROV guidance, weapon launch systems,
ship navigation and control
mobile mapping
train positioning (GPS dead reckoning)
MWD – drilling guidance

MS1010L PARAMETERS

All values are specified at ambient temperature (20°C) and at 3.3 V supply voltage V_{DD}, unless otherwise stated. Acceleration values are defined for differential signal (OUTP-OUTN).

Parameter	Comments	Min	Typ.	Max	Unit
Accelerometer					
Full scale		±10			g
Non-Linearity	IEEE Norm, % of full scale		0.3	1.0	%
Frequency response	-3dB	100			Hz
Resonant frequency			4		kHz
Noise	in band		34		µg/√Hz
Resolution	@ 1Hz		34		µg rms
Startup time	Sensor operational, delay once POR triggered		40		µs
Bias (K0)					
Nominal	Calibration accuracy	-34		34	mg
Temperature coefficient	See glossary	-2	±0.5	2	mg/°C
Long term bias repeatability at 20°C	@1'000g - See glossary		1.5		mg
	@6'000g - See glossary		7.5		mg
In-run bias stability	Based on Allan Variance characterization (@ 10s)		15		µg
TurnON - TurnON	See glossary		75		µg
Scale factor (K1)					
Nominal	Calibration accuracy	266	270	274	mV/g
Temperature coefficient	See glossary	20	120	220	ppm/°C
Long term scale factor repeatability at 20°C	See glossary		300		ppm
Axis misalignment	See glossary K_p, K_h		3		mrad
Self-test					
Frequency	Square wave output		24		Hz
Duty cycle			50		%
Amplitude	Peak to peak		1		g
Input threshold voltage	active high	80			% V_{DD}
Temperature sensor					
Output voltage @20°C		1.20	1.23	1.26	V
Sensitivity			-4		mV/°C
Output current load				10	µA
Output capacitive load				10	pF
Reset					
Input threshold voltage	active low			20	% V_{DD}
Power requirements					
Supply voltage (V_{DD})		3.2	3.3	3.4	V
Supply current (I_{DD})			2.3	4	mA
Accelerometer outputs					
Output voltages	OutP, OutN over full scale	0.14		3.16	V
Differential output	Over full scale		±2.7		V
Resistive load		1000			kΩ
Capacitive load				100	pF

Table 3: MS1010L Specifications

Absolute maximum ratings

Absolute maximum ratings are stress ratings. Stress in excess of the environmental specifications in the datasheet can cause permanent damage to the device. Exposure to the maximum ratings for an extended period of time may degrade the performance and affect reliability.

Parameters	Comments	Min.	Max.	Unit
Supply voltage Vdd		-0.3	+3.9	V
Voltage at any pin		-0.3	Vdd+0.3	V
Temperature	Operational	-40	125	°C
	Storage	-55	125	°C
Vibration	Random / 20 – 2'000 Hz		20	g rms
Shock	0.15 ms, half sine, single shock, not repetitive, in one direction		6'000	g
ESD stress	HBM model	-1	1	kV

Table 7: Absolute maximum ratings

MS1010L: Typical initial performances on multiple sensor at 3.3 VDC supply voltage (V_{DD}) and ambient temperature for all graphs, unless otherwise stated (multiple sensor: multiple color line , min/max: red line , typical value: green line).

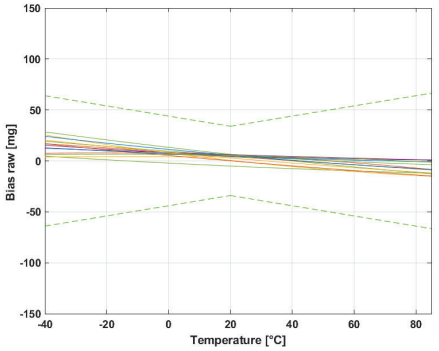

Figure 13: Raw bias

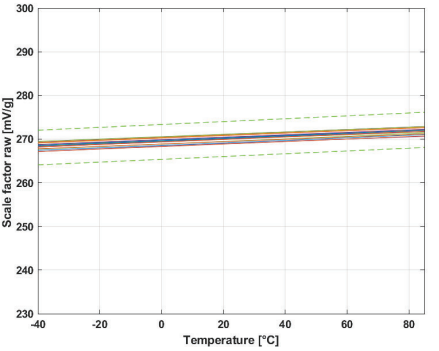

Figure 14: Raw scale factor

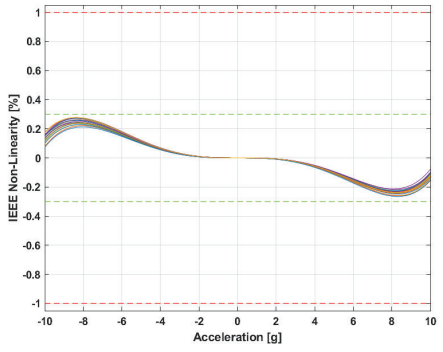

Figure 15 : Non-linearity IEEE

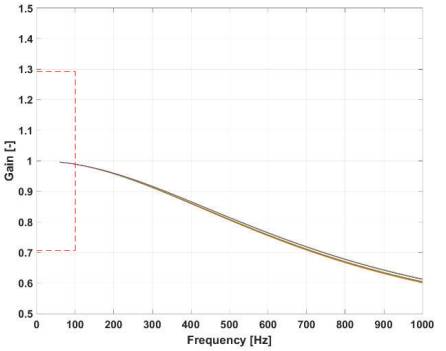

Figure 16 : Frequency response

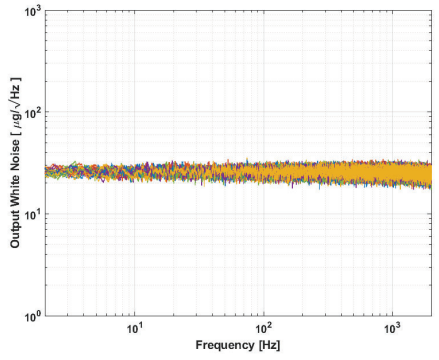

Figure 17: Typical white noise

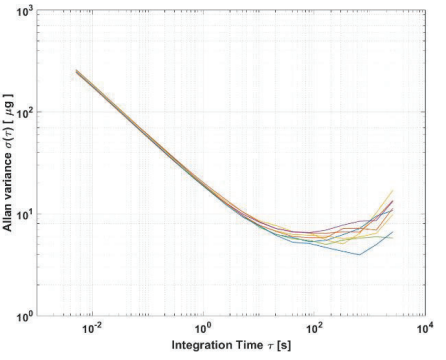

Figure 18: Allan Variance

Bibliography

Anon (2014). "Guide to comparing gyro and imu technologies – micro-electro-mechanical systems and fiber optic gyros". URL: kvh.com (visited on 2022-09-30).

Dengwei, Z., Z. Yuxiang, S. Xiaowu, L. Cheng, F. Wenlan, and Z. Wenqing (2013). "Magnetic drift in single depolarizer interferometric fiber-optic gyroscopes induced by orthogonal magnetic field." *Optical Engineering* **52**:5, pp. 1–5. ISSN: 00913286.

Jurado, J., C. Schubert Kabban, and J. Raquet (2019). "A regression-based methodology to improve estimation of inertial sensor errors using allan variance data." *Navigation* **66**:1, pp. 251–263.

Markley, F. L. and J. L. Crassidis (2014). *Euler Angles.* Vol. 33. Space Technology Library. 33. Springer New York. ISBN: 978-1-4939-0801-1.

Morris, T., A. Zawada, D. Garcia, J. Wheeler, and M. Digonnet (2022). "Optimization of the angular random walk in laser-driven fiber-optic gyroscopes." *IEEE Sensors Journal* **22**:3, pp. 2205–2212.

Naser, E.-S. and Y. Ahmed (2020). "Inertial sensors technologies for navigation applications: state of the art and future trends." *Satellite Navigation* **1**:1, pp. 1–21. ISSN: 2662-1363.

National Geospatial-Intelligence Agency (2014). *National geospatial-intelligency agency (nga), standardization document*. Version 1.0.0.

Noureldin, A., D. Irvine-Halliday, H. Tabler, and M. Mintchev (2001). "New technique for reducing the angle random walk at the output of fiber optic gyroscopes during alignment processes of inertial navigation systems." *Optical Engineering* **40**:10, pp. 2097–2106.

Saab AB (2022). *Saab fiber optic gyro products*. URL: https://www.saab.com/products/fiber-optic-gyro-products (visited on 2022-09-15).

Savage, P. G. (2015). *Computational elements for strapdown systems*. Originally published in NATO Research and Technology Organization (RTO) Sensors and Electronics Technology Panel (SET) Low-Cost Navigation Sensors and Integration Technology RTO EDUCATIONAL NOTES RTO-SET-116(2008), Section 9. Published in 2009. URL: http://www.strapdownassociates.com/Computational%20Elements.pdf (visited on 2023-01-13).

Savage, P. G. (1997). *Strapdown inertial navigation lecture notes*. Prepared by Strapdown Associate INC. as part of lecture series. Sixth printing.

Tazartes, D. (2014). "An historical perspective on inertial navigation systems." *2014 International Symposium on Inertial Sensors and Systems (ISISS), Inertial Sensors and Systems (ISISS), 2014 International Symposium on*, pp. 1–5. ISSN: 978-1-4799-0916-2.

Titterton D. H., W. J. L. (2004). *Strapdown Inertial Navigation Technology, second edition*. The American institute of Aeronautics and Astronautics, The Institution of Electrical Engineers, Herts, United Kingdom.

Vali, V. and R. W. Shorthill (1976). "Fiber ring interferometer." *Applied Optics* **15**:5, pp. 1099–1100. ISSN: 1559128X.

Woodman, O. J. (2007). *An introduction to inertial navigation*. Tech. rep. University of Cambridge, computer labaratory.

Lund University
Department of Automatic Control
Box 118
SE-221 00 Lund Sweden

Document name
MASTER'S THESIS

Date of issue
June 2023

Document Number
TFRT-6196

Author(s)
Tim Djärf

Supervisor
Karl-Johan Krantz, SAAB Aktiebolag, Sweden
Bo Bernhardsson, Dept. of Automatic Control, Lund University, Sweden
Karl-Erik Årzén, Dept. of Automatic Control, Lund University, Sweden (examiner)

Title and subtitle
Practical Trials of Fiber Optical Gyroscope Based Inertial Navigation System

Abstract

There exists a need for inertial navigation systems within a multitude of applications, such as drones, unmanned vehicles, and guidance systems. Saab produces gyroscopes for stabilization purposes, but the gyroscopes could also be used as part of an inertial navigation system. This thesis investigate the viability of using the hardware and software that Saab already uses, with the addition of accelerometers which is sourced from Safran sensing technologies; as components in a inertial navigation system.

A prototype inertial navigation system has been built, and a navigation algorithm has been implemented. The prototype has been calibrated on both sensor and system level. The sensors have been verified to lie well within the manufacturers specifications.

It is possible to use the current hardware used by Saab for navigation purposes, as verified by measuring timing and computational load of the prototype system. However, there still exist a numerical error for the velocity and position calculation which requires additional development. Development and testing of the navigation unit will have to be continued outside the scope of this master's thesis to determine how viable the system could be as a product used in actual applications.

Keywords

Classification system and/or index terms (if any)

Supplementary bibliographical information

ISSN and key title
0280-5316

ISBN

Language
English

Number of pages
1-66

Recipient's notes

Security classification

http://www.control.lth.se/publications/